2-6-2018

Geologic Framework of the Fang Hot Springs Area with Emphasis on Structure, Hydrology, and Geothermal Development, Chiang Mai Provence, Northern Thailand

Spencer H. Wood
Boise State University

Pichet Kaewsomwang
Chiang Mai University

Fongsaward Suvagondha Singharajwarapan
Chiang Mai University

Wood *et al. Geotherm Energy (2018) 6:3*
https://doi.org/10.1186/s40517-017-0087-7

Geothermal Energy

RESEARCH

Open Access

Geologic framework of the Fang Hot Springs area with emphasis on structure, hydrology, and geothermal development, Chiang Mai Province, northern Thailand

Spencer H. Wood[1*], Pichet Kaewsomwang[2,3] and Fongsaward Suvagonda Singharajwarapan[2]

*Correspondence: swood@boisestate.edu
[1] Department of Geosciences, Boise State University, 1910 University Drive, Boise, ID 83725, USA
Full list of author information is available at the end of the article

Abstract

Geologic mapping, a magnetotelluric survey, well data, and earlier reports are integrated to guide further development of the Fang geothermal system. The Fang Hot Springs originally flowed ~ 20 l s^{-1} of 90–99 °C water from a 10-hectare area of crystalline rocks presumed to be of Triassic age. Four wells 92–500 m deep now flow ~ 20 l s^{-1} of 110–115 °C water and generate 115–250 kWe from the 1989 Ormat binary power plant. Wells are not pumped nor is the spent water re-injected. Temperatures of 130 °C occur in some wells and water chemistry indicates reservoir temperatures of 150 °C. The springs now flow ~ 10 l s^{-1}. The Fang geothermal area is at the west end of the active left-lateral strike-slip Mae Chan fault (MCF). MCF transitions to extensional faulting along the western boundary of the Cenozoic Fang basin. The hot waters emanate from crystalline rocks 0.7 km north of the MCF. Permeable fractures may be tensile fractures at the right-stepping fault tip. The less permeable MCF fault core and Cenozoic sediments of the Fang basin to the SW are not considered to be drilling targets. Unrelated to the fracture system is the Doi Kia detachment fault which places Paleozoic sediments over crystalline rock with a low-angle contact. Electrical resistivity surveys detect low resistivity (< 60 Ωm) only within the upper 50–100 m of the hot springs area. Deeper crystalline rock is > 100 Ωm. Low resistivity is caused mostly by conductive minerals of hydrothermal alteration, and not by the geothermal water of resistivity 5.6 Ωm. No deep resistivity anomaly is detected beneath the seeps or producing wells, although resolution of past surveys would not have imaged narrow zones of alteration. High-resolution resistivity surveys focused on detecting the deeper fracture system are recommended over the hot well area and south over the area underlain by crystalline rocks. Future development should focus on drilling wells (≤ 500 m) with diameters large enough to install submersible pumps to increase flows. Development of several MWe may be possible and should include a designed re-injection well system to sustain pump levels.

Keywords: Fang geothermal system, Thailand, Structural geology, Strike-slip fault, Crystalline rocks, Resistivity, Hydrology, Geothermal development

Background

In northern Thailand, the 16 hot springs systems identified with surface temperatures > 80 °C are mostly associated with granitic rocks and faults active during the Quaternary. Only the Fang Hot Springs and San Kamphaeng Hot Springs have proven 130 °C water flows from wells (Singharajwarapan et al. 2012; Wood and Singharajwarapan 2014). The Fang Hot Springs geothermal system was drilled and developed for the generation of electricity in 1989 (Ramingwong et al. 2000) and is being considered for further development. Important to further development of the Fang Hot Springs geothermal area is an understanding of the fault system geometry that conducts hot water to the surface. Ideally, for future drilling, we would like to know the location, strike and dip, and width of the main fracture conduits for hot water. In this paper we describe the structural geology of the hot springs, incorporate results of direct current (DC) and magnetotelluric (MT) resistivity surveys, document the wells and seeps, and make recommendations for further development.

The geothermal system was initially investigated by EGAT (Electricity Generating Authority of Thailand), Chiang Mai University Geological Sciences, and several foreign research groups in the 1970s and 1980s. Successful wells that were drilled in the 1980s and 1990s collectively produced 22 l/s of 125 °C water. A 300 kW binary organic Rankine cycle (ORC) power plant was installed in 1989. A new round of exploration of northern Thai geothermal resources was initiated in 2010 funded by the Thailand Department of Alternative Energy Development and Efficiency (Singharajwarapan et al. 2012). ORMAT Corporation examined the geothermal systems of northern Thailand for potential siting of power plants (Owens 2012). The Thailand Department of Groundwater Resources funded investigations by Chiang Mai University, Mahidol University, and Panya Consultants, Ltd. in 2013. Focus of these studies was to locate a site for drilling new wells for electrical power generation. This paper presents a compilation of data, new geological mapping in the Fang area, and recommendations for future exploration.

Non-magmatic geothermal systems in granitic rocks are common, but few systems are reported with the high water temperatures and flows as those that occur at Fang (130 °C and flow > 20 l s^{-1}). For example, the hottest springs in the Idaho batholith (Bonneville Hot Springs and Boiling Springs) are < 88 °C and flows < 23 l s^{-1} (Ross 1971; Mayo et al. 2014).

Geology and geothermal setting of the Fang Basin

Geology of the Fang Basin

Basement rocks of the Fang Basin are a part of the Inthanon zone, an accretionary complex of Paleozoic Paleo-Tethys ocean rocks thrust westward over the eastern flank of the Sibumasu block (Ridd 2015; Ridd et al. 2011) (Fig. 1). The hot springs at Fang emanate from fractures in foliated granite of the basement rocks north of the active Mae Chan fault. A number of geologic maps have been made of the area, but there was little agreement on location and nature of contacts, and no discussion of evidence for faults (von Braun and Hahn 1981; Chaturongkawanich et al. 1980; Imsamut and Krawchan 2005). Detailed proprietary drilling and seismic information on the Cenozoic structure of the Fang Basin oil fields has been obtained by the Defense Minerals Agency, some of which

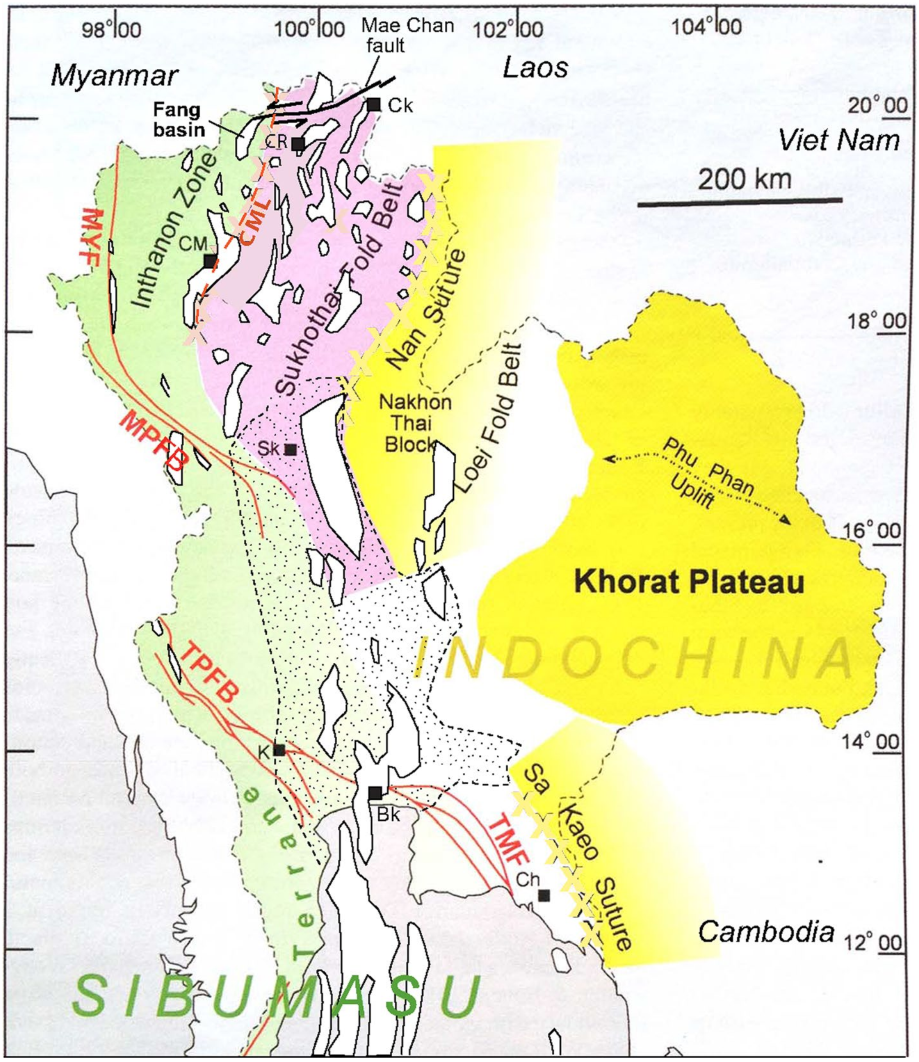

Fig. 1 Tectonic map of Thailand showing major terranes and structural provinces modified after Ridd et al. (2011). Major tectonic lines shown in red are *MYF* Mae Yuam fault; *MPFB* Mae Ping fault belt; *TPFB* Three Pagodas fault belt; *TMF* Tha Mai fault; *CML* Chiang Mai line. Cenozoic rift basins shown in outlined white color after Uttamo et al. (2003). *Bk* Bangkok; *Ch* Chanthaburi; *CK* Chiang Khong; *CM* Chiang Mai; *CR* Chiang Rai; *K* Kanchanaburi; *Sk* Sukhothai

is published by Settakul (2009) and Kongmongkhol and Chantraprasert (2015), but most of the data are unavailable to the public.

West of the Fang Basin is an N–S trending belt of west-dipping, folded, Paleozoic sedimentary rocks extending west beyond the Myanmar border (Figs. 2, 3). Imsamut and Krawchan (2005) estimate a thickness of 2900 m for this Paleozoic section. This N–S trending belt of Cambrian through Permian sediments is not cut or offset by the Mae Chan fault (Figs. 2–4).

The Paleozoic sedimentary rocks are in fault contact with foliated granitic rocks and gneiss. Cobbing (2011) called these rocks "northern Thai "S-type" granites of the central province". Age is controversial. Some foliated crystalline rocks were earlier thought to be

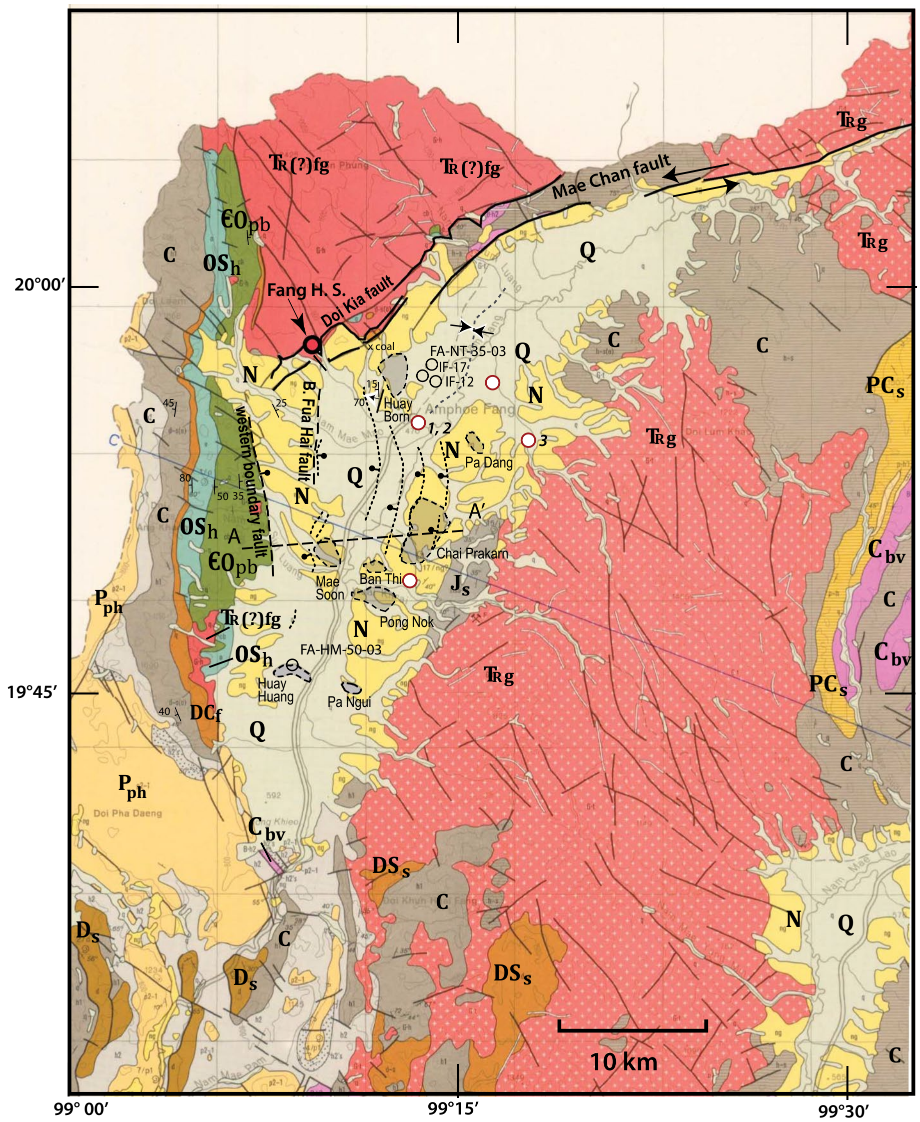

Fig. 2 Geologic map of the Fang Basin area from von Braun and Hahn (1981) showing location of Fang Hot Springs. Formation names from Imsamut and Krawchan (2005) and the Thailand Department of Mineral Resources (2013). We recognize that mapping since 1981 has somewhat changed the outcrop areas and assigned ages. Solid lines are faults related to Fang geothermal area, dotted lines are subsurface faults mapped by Kongmongkhol and Chantraprasert (2015). Symbols explained in Fig. 3

emplaced during Carboniferous time (Imsamut and Krawchan 2005, p. 118) but are now regarded as Permo-Triassic. Mapped on the north side of Fang Basin is unfoliated biotite granite of Triassic age (Imsamut and Krawchan 2005, p. 109) containing either pendants or fault slivers of early Paleozoic rocks. Crystalline rocks of Inthanon zone yield zircon dates younger than Permian, and most are late Triassic or younger, emplaced or metamorphosed in the Indosinian orogeny (Cobbing 2011). The few earlier ages on zircon cores are interpreted as protoliths of the granitic rocks of the Sibumasu terrane (Gardiner et al. 2016). Mylonitic textures within the stressed granite suggest that the Paleozoic sediments resting on the foliated crystalline rocks may be low-angle detachments, similar to those described in the Chiang Mai basin by Morley et al. (2011).

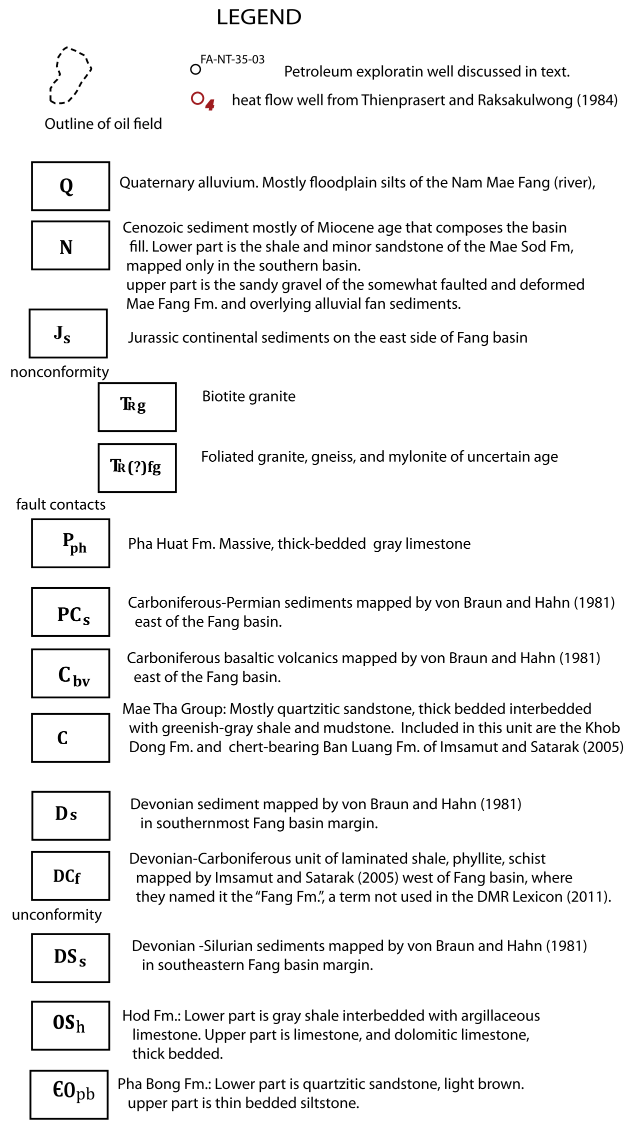

Fig. 3 Legend for geologic map of Fig. 2 with explanation of geologic map units and symbols for oil fields and wells

The east side of the Fang Basin is mostly Triassic unfoliated porphyritic granite intrusive into Carboniferous sediments and overlain by Jurassic continental sediments (von Braun and Hahn 1981; Imsamut and Krawchan 2005). No new zircon ages have been published for granitic rocks about the Fang Basin. Ages for unfoliated granite to the north and south generally range 205–220 Ma, and are interpreted as magmatism associated with the Late Triassic closure of the Paleo-Tethys ocean, collision and suturing of the Sibumasu block with the Indochina block along the "Chiang Rai line" (Gardiner et al. 2016).

Fang Basin is an NE–SW-trending basin, 60 km long and about 18 km wide at mid-basin. The basin is a half-graben bounded on the west with an upward-concave, ~ 25° east-dipping, normal fault (Morley and Racey 2011, p. 226; Settakul 2009; Nuntajun

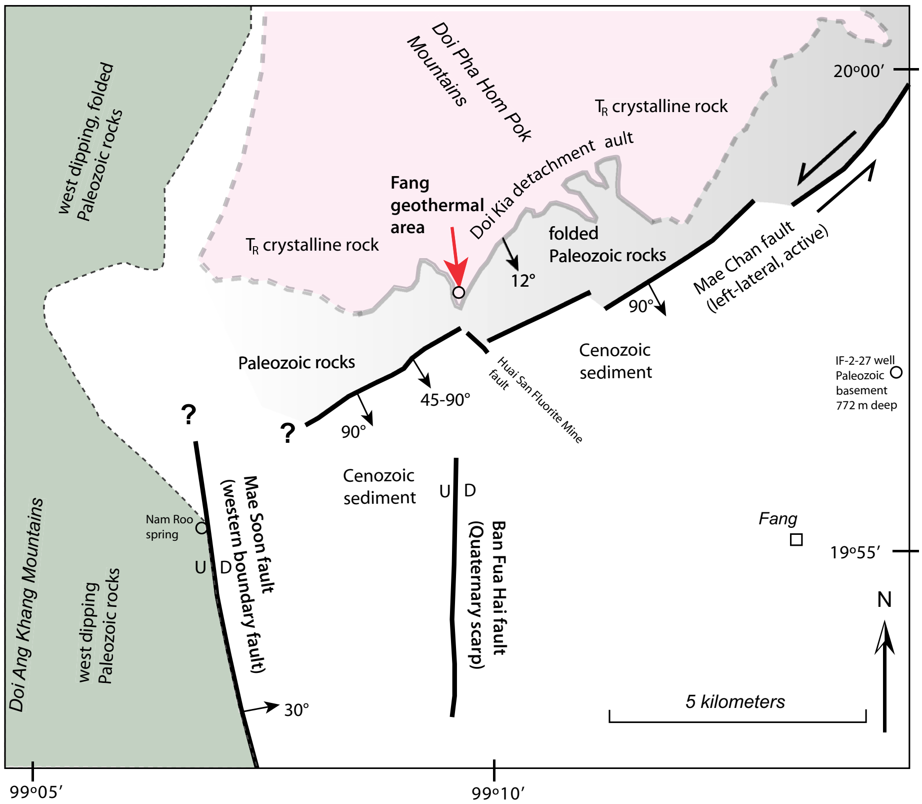

Fig. 4 Map showing fault relationships in the Fang basin at the west end of the Mae Chan fault

2009; Kongmongkhol and Chantraprasert 2015) (Fig. 5). Deposition in the basin is thought to be late Oligocene through the Pliocene. Cenozoic sediment extends to 2800–3000 m depth. Morley and Racey (2011) interpret folding of the Mae Fang Formation (L. Miocene to Pliocene) along the western boundary fault as a basin inversion structure (Fig. 5). The western boundary fault occurs at the western edge of rolling foothills, at the foot of rugged mountains of Paleozoic sedimentary rocks which lay to the west (Fig. 6). The foothills are underlain by moderately deformed late Cenozoic sediment, the Mae Fang Formation, or the younger deformed alluvial fan deposits, both of which are mapped by von Braun and Hahn (1981) as Neogene sediments shown as "N" in Figs. 2, 3.

Oil seeps have been known for many years in the Fang Basin, near the present Chai Prakarn field (Figs. 2, 3). Over 240 wells have explored the Cenozoic basin sediments for petroleum. Principal producing reservoirs are fluvial and deltaic sands within dark gray claystone and oil shale of the Miocene Mae Sot Formation (Fig. 7). The producing sands of the Mae Soon field are mostly at 660–820 m depth. Total production from 5 main fields has been about 7 million barrels of 30–40 API gravity, high paraffin oil (Settakul 2009).

Structure at the northwestern end of the basin must be affected by the east termination of the NE–SW-trending strike-slip Mae Chan fault and N–S trending normal faults in the basin sediments (Fig. 4). Active left-lateral motion on the Mae Chan fault (Fenton et al. 2003; Weldon 2015) suggests that the SE block (i.e., Fang Basin) is pulling apart, moving to the northeast, thereby causing normal faulting.

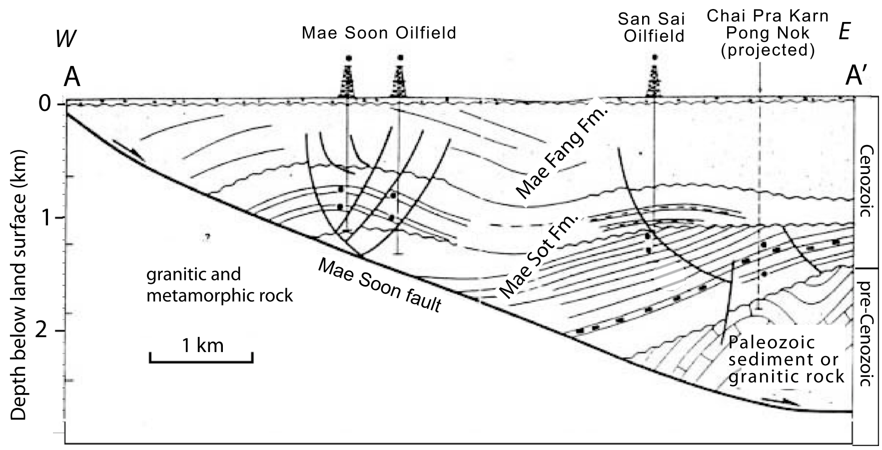

Fig. 5 Cross section of the southern Fang basin from Settakul (2009). Location of section shown on Figs. 2, 3. The section, based on proprietary seismic reflection profiles, shows the low-angle normal fault ("Mae Soon fault") along the western boundary of the basin. Black dots indicate proven or potential petroleum traps

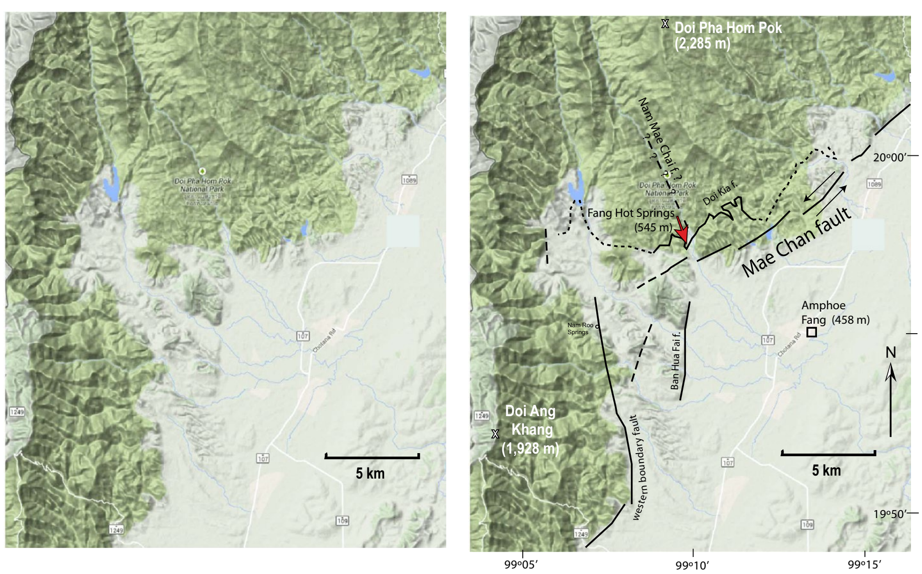

Fig. 6 Relief map of the northern Fang basin showing physiographic expression of the late Cenozoic faults

The Fang basin has similar geometry (i.e., the mirror image) to the La Tet right-lateral fault and the Cerdanya basin in the eastern Pyrenees (Cabrera et al. 1988; Gabàs et al. 2016). Mann (2007) has classified this type of basin bounded on one side by a single strike-slip fault as a "fault termination basin" to distinguish it from classical pull-apart basins which are confined by two sub-parallel strike-slip faults.

Geothermal gradients

Of interest are the regional geothermal gradients in crystalline rocks of the Fang area that might be extrapolated to depth, to understand the depth of circulation of the 130 °C hot water. Temperature profiles in the hot springs area are from shallow wells in

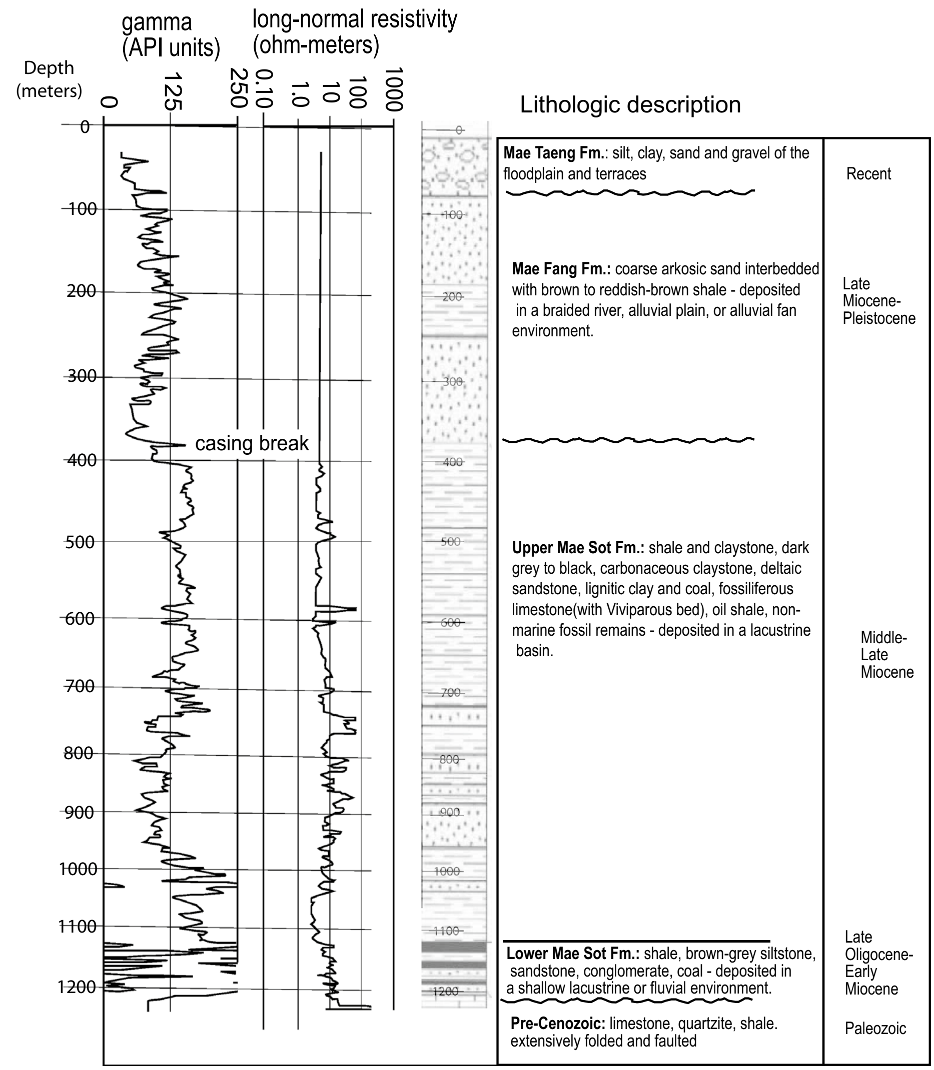

Fig. 7 Geophysical logs and stratigraphy of the Cenozoic basin sediment in well FA-HM-50-03 in the southern Fang basin (location shown in Figs. 2, 3) (after Giao et al. 2011). Resistivity log shows the low resistivity (~ 6 Ωm) of the upper 300 m of the clayey Mae Sot Formation

crystalline rock (Fig. 8), clearly heated by convective flows and are not useful for predicting the depth of circulation. High gradients (74–133 °C/km) are measured in shallow petroleum wells in the of the Fang basin sedimentary rocks and these measurements are often cited as the regional gradient. These high gradients are not observed in the one available deep well (FA-HM-50-03) measurement of 32.8 °C/km and this discrepancy prompts this review of the temperature-depth profiles for the area (Fig. 8).

Crystalline rock geothermal gradients

Temperature profiles of the shallow geothermal wells (FGTE-6, FGTE-8, and FGTE-10) in crystalline rocks are reported by Wanakasem and Takabut (1986). These profiles (Fig. 8) show temperature inversions caused by shallow, high-temperature, fracture flows. Below these peaks in temperature the temperatures decrease. Inversion profiles are common in geothermal wells (Bodvarsson 1973; Ziagos and Blackwell 1986). These

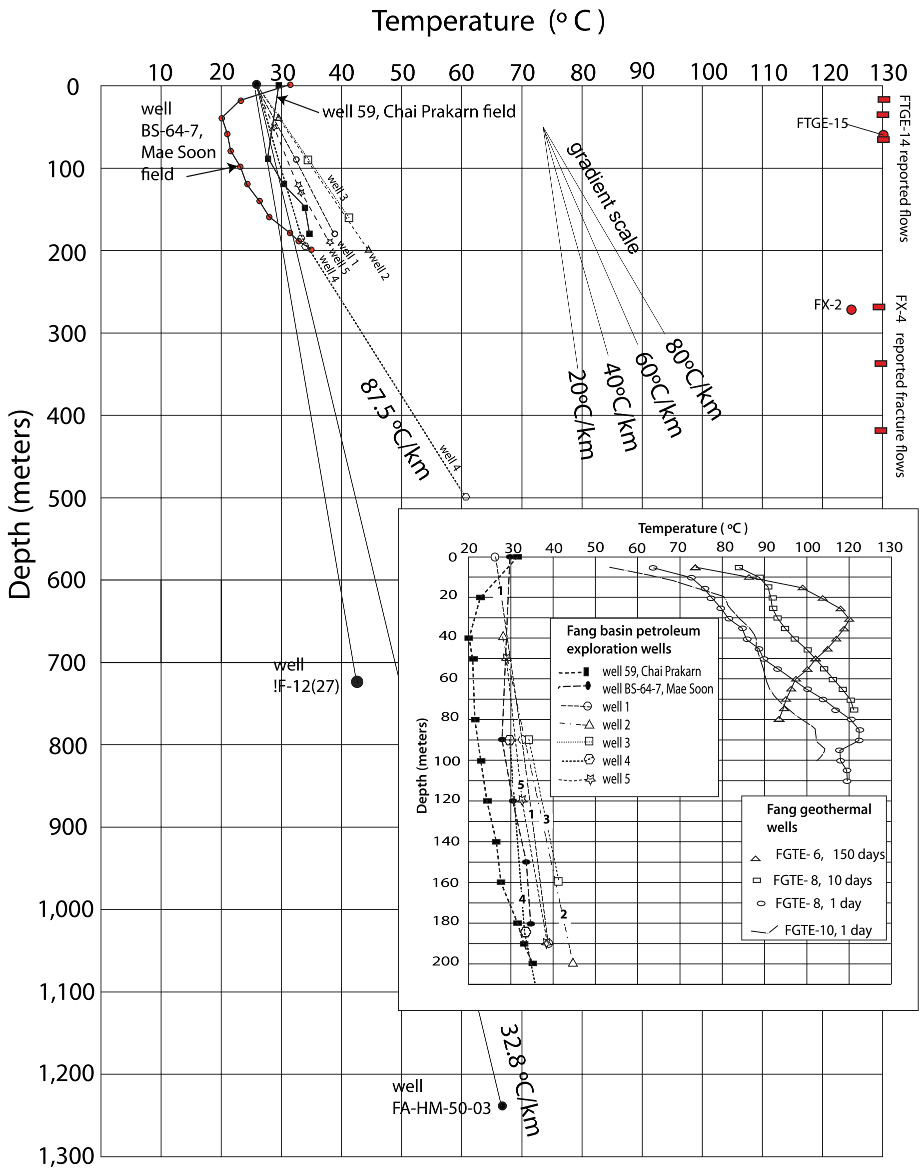

Fig. 8 Temperature-Depth plot showing reported geothermal gradients of petroleum exploration wells in Fang basin sediments and an inset figure showing the only available temperature logs of geothermal wells in crystalline rocks. Large plot: Solid lines connect measurement points (solid dots) of Barr et al. (1979) from wells which are located in oil fields shown in Figs.2, 3 (detailed locations were not published). Dashed lines are gradients in wells (locations in Figs. 2, 3) published by Thienprasert and Raksaskulwong (1984), which we extrapolate upward to an assumed surface temperature of 26 °C. (Because these authors did not publish temperatures, we attempt to reconstruct a profile using their published gradients.) Drill-stem test temperature of 66.5 °C at 1240 m in well FA-HM-50-03 is from Giao et al. (2011). Bottomhole temperature of well IF-12(27) is an unpublished log considered low because it was probably logged shortly after drilling. Selected temperatures of producing geothermal wells shown by symbols on upper right margin (symbols placed at depths of producing fractures) (see Table 1). Inset plot: Temperature logs of geothermal wells (locations shown in Fig. 23 and in Table 1) made 1–150 days after drilling (from Wanakasem and Takabut (1986)) and detail of profiles from wells in sedimentary rocks duplicating those shown in upper left of large plot. Temperature inversions in the geothermal wells are discussed in text

wells, affected by convection, do not provide information on the regional conductive gradient in crystalline rocks at Fang. We know of only one deep measurement in biotite granite reported by Wood et al. (2016) for a borehole at Muang Rae, 120 km southwest of

Table 1 Wells drilled in the Fang geothermal area

Well name	Depth (m)	Tflow	Tmax	Flow ($l\ s^{-1}$)	Open hole depth (m)	Open hole diameter (cm)	Surface csg. diam. (cm)/depth (m)	Type csg. OD/ID (cm)	Lower csg. Diam. (cm)/depth (m)	Type csg. OD/ID (cm)	Well head press. (bars)	Source	Remarks	WGS84 easting	WGS84 northing	Date drilled
FTGE-1	29 (br), 30 (c)		100 (c), 110 (br)		30							c, wt, br	110° at 25 m, intermittant shooting flow 30-m high, well collapsed (br)	16.325*	7.813*	5/1982
FTGE-2	80		37				20.32/13.75					c, wt, br		16.425*	7.500*	6/1982
FTGE-3	94	98	111.8	1.0–2.0	80	17.145	20.32/14	21.91/20.247				c, wt, br	111.8° at bottom, flow includes small amount of steam (br)	16.309	7.754	8/1982
FTGE-4												c, wt, br	Eruption of water occurred before casing set, well collapsed (br)	16.235*	7.645*	1982 (?)
FTGE-5	19.6	105	115	2.0–4.0	13.1	17.145	20.32/6.5	21.91/20.247				c, wt, br	Max temp after closing well 20 min (br), presently marked by 1.5 m brick outline (ki)	16.236	7.654	Before 1986
FTGE-6	85.4		122.3 (c), 93.7 (wt)	None	56	14.287	20.32/6.75	21.91/21.156	15.24/29.4	16.61/15.64		c, wt	"Dry hole"(wt). Not located in 2015. Temperature log (Fig. 8)	16.340*	7.835*	Before 1986
FTGE-7	52.7	105	130.2 (br) 118 (wt)	3.80	35	14.287	20.32/7	21.91/21.156	15.24/17.7	16.61/15.64		c, wt	Not used for power. Shut in for 30 min. intervals, and then geysers 35 m high (ki)	16.061	7.643	Before 1986
FTGE-8	120	105	130 (c) 122 (wt)	0.20	96	14.287	20.32/7.2	21.91/21.156	15.24/24	16.61/15.64		c, wt	Temperature log (Fig. 8)	16.142*	7.515*	Before 1986

Table 1 continued

Well name	Depth (m)	Tflow	Tmax	Flow ($l\ s^{-1}$)	Open hole depth (m)	Open hole diameter (cm)	Surface csg. diam. (cm)/depth (m)	Type csg. OD/ID (cm)	Lower csg. Diam. (cm)/depth (m)	Type csg. OD/ID (cm)	Well head press. (bars)	Source	Remarks	WGS84 easting	WGS84 northing	Date drilled
FTGE-9	64	105	128.5 (c) 123 (wt)	0.60	34	14.287	20.32/11.5	21.91/21.156	15.24/30	16.83/15.48		c, wt		16.073	7.625	Before 1986
FTGE-10	103.3		118.4 (c) 115 (wt)	None	79.3	14.287	20.32/2	21.91/21.156	15.24/24	16.83/15.49		c, wt	location uncertain, said to be up on hill north of large tree above FTGE-15 (ki). Temperature log (Fig. 8)			Before 1986
FTGE-11	58.8	105	125 (c) 118 (wt)	0.50	40.8	14.287	20.32/7	21.91/21.157	15.24/18	16.83/15.50		c, wt	Intermediate flow	16.286	7.704	Before 1986
FTGE-12	43.7	105	128.1 (c) 115 (wt)	4.01	37.7	14.287	20.32/6.5	21.91/21.158	15.24/6	16.83/15.51		c, wt	Steady flow	16.218	7.624	Before 1986
FTGE-13	90	105	115.8	1.00	72	14.287	20.32/6	21.91/21.159	15.24/18	16.83/15.52		c,	Intermediate flow	16.253	7.667	Before 1986
FTGE-14*	73.2 (c) 92 (ki)	110	131.6	7.94	64.2	14.287	20.32/6	21.91/21.160	15.24/9	16.83/15.53	1.5	c,	Steady flow (c), said to be 92 m deep with hot water inflow at 18 m/38 m/66 m (ki). Also called the "Khun Theptorn well"	16.081	7.595	1985–86
FTGE-15*	60.5 (c), 160 (ki)	121	130.6	13.97	52.5	14.287	20.32/6	21.91/21.161	15.24/8	16.83/15.54	1.5	c,	Said to be 160 m deep with hot water inflow at 60 m (ki). Also named "Khun Wichian well"	16.058	7.678	1985–86
FTGE-16	~100 (ki)												No information	16.205	7.910	1986
FX-1	500		108	None								tk	Location unknown			1995 (?)

Table 1 continued

Well name	Depth (m)	Tflow	Tmax	Flow ($l\ s^{-1}$)	Open hole depth (m)	Open hole diameter (cm)	Surface csg. diam. (cm)/depth (m)	Type csg. OD/ID (cm)	Lower csg. Diam. (cm)/depth (m)	Type csg. OD/ID (cm)	Well head press. (bars)	Source	Remarks	WGS84 easting	WGS84 northing	Date drilled
FX-2	500	125									1.5	tk	Fracture zone at 270 produces 6.94 l/s of 125 °C	16.177	7.404	1995 (?)
FX-3	500		113	None								tk	Location unknown			1995 (?)
FX-4	500		130									tk	Fracture zones at 268, 337, and 417 m. (tk) indicates a total flow of 10 l/s, but inclear if this is a total of FTX-2 and FTX-4	16.251	7.658	1995 (?)
BH-3	18	100	110	1.00	14	7.302	7.62/4	10.16/9.012				c, wt, br	Steady flow (wt)	16.213*	7.798*	6/1984
BH-4	34.7	100	124	0.50	27.7	7.302	10.16/7	11.43/10.22			0.85	c, wt, br	Steady flow (wt)	16.038*	7.765*	6/1984
BH-8	25	104	110	1.50	12.2	7.302	8.89/12.8	10.16/9.012				c, wt, br	Steady flow (wt)	16.285*	7.846*	6/1984
BH-11				1.00								wt	Steady flow (wt), location unknown			6/1984
2 wells												ki	2 wells, 5 m apart near sign (Ing-Doi camp)	16.130	7.956	?
Bo Luang Camp												ki	This might be BH-3 or BH-8	16.213	7.798	?

(br) Ratanasthien et al. (1985), (c) Chuaviroj (1987). (wt)Wanakasem and Takabut (1986). (tk) Korjedee (2000). (ki) Khun Inton, EGAT staff at Fang, personal communication, 2015

note that Chuaviroj (1987) reports higher maximum temperature than does Wanakasem and Takabut (1986)

* Asterisk on UTM location indicates it has been scaled from scans of maps by Coothungkul and Chinapongsanond (1985) and Wanakasem and Takabut (1986)

Fang. The lower part (850–1000 m depth) of that borehole shows a gradient of 23.3 °C/km. A heat flow of 70 m Wm^{-2} is calculated for the Muang Rae field, assuming a granite conductivity of 3.0 W m^{-1} $°C^{-1}$.

Fang sedimentary basin geothermal gradients

High geothermal gradients (74–133 °C/km) and high heat flow (68–168 mWm^{-2}) are reported over much of the Fang basin in the shallow sediments (< 500 m) (Barr et al. 1979; Thienprasert and Raksaskulwong 1984), and these high values are commonly cited in recent literature (Racey 2011; Petersen et al. 2006). Very few measurements have been made available from deeper wells, but a drill-stem-test temperature recorded on the FA_HM_50-03 well in the southern Fang basin (Figs. 2, 3) is considered reliable (not affected by drilling). That temperature at depth 1240 m is 66.5 °C (Giao et al. 2011) which indicates a much lower gradient (32.8 °C/km) than reported in earlier publications. Thienprasert and Raksaskulwong (1984) report gradients without temperature values on five wells in Fang basin sediments. In order to represent their data in Fig. 8, we have extrapolated their gradient values to an assumed mean annual surface temperature of 26 °C. Locations of their 5 wells are shown in Figs. 2, 3. They generally show gradients of ~ 87 °C/km. Barr et al. (1979) measured gradients in two wells at the Mae Soon and the Chai Prakarn oil fields (Fig. 8). For the deeper parts of their ~ 200-m-deep wells, the gradients are 74–133 °C/km. They reported surface temperatures higher than 26 °C, and low temperature inversions ~ 20 °C in the upper 50–100 m on the two wells, presumably caused by hot summer days and by cool, shallow groundwater flow, respectively. Because of the discrepancy between high gradients in the shallow sedimentary section, and lower gradients in the deep well, we examine the sources of heat flow that may contribute to the geothermal areas of northern Thailand.

Heat flow to estimate the geothermal gradient in crystalline rock

Heat flow (mW m^{-2}) is a calculated value: $q = k{\cdot}(\Delta T/\Delta z)$, where k is thermal conductivity (W m^{-1} $°C^{-1}$) and $\Delta T/\Delta z$ is the geothermal gradient (°C m^{-1}). Thermal conductivity of granite is typically 2.9–3.2 W m^{-1} $°C^{-1}$. Geothermal gradients are typically high in sedimentary basins because of the low thermal conductivity of sediments (1.3–1.7 W m^{-1} $°C^{-1}$). Thus for the same heat flow value, the gradient in crystalline rocks will be about 1/2–2/3 of that of the gradient in sediments. Heat flow is anomalously high (78–101 mW m^{-2}) in the extensional basins of northern and central Thailand and in the Gulf of Thailand (Morley and Westaway 2006; Madon 1997). These high values are in comparison to a lower regional heat flow over much of Thailand of 42–63 mW m^{-2} (Thienprasert and Raksaskulwong 1984). The heat source for Fang geothermal area is from radioactive decay of naturally occurring K, Th, and U in the crustal rocks of the area and lesser amounts of those elements in the earth's mantle. The northern Thai geothermal systems are not associated with volcanic or underlying magma systems. Using measured heat generation from crystalline rocks of the area (Table 2) from Kawada et al. (1987) and estimated amounts from the lower crust, mantle lithosphere, and the asthenosphere. We estimate surface heat flow in Table 3 between 48 and 109 mW m^{-2}, and a value of 75 mW m^{-2} using average values of each contribution. These estimates show reasonable agreement, but are somewhat lower than the values of heat flow measured in

Table 2 Heat production of crystalline rocks at Fang

Sample no.	Rock type	Th (ppm)	U (ppm)	K (%)	Heat production (μW m)$^{-3}$
KK-FANG-1	Orthogneiss	17.5	3.3	2.14	2.26
KK-FANG-2	Mylonite	27.6	6.5	3.30	3.89
MS-82Y2501	Mylonite	15.1	11.4	4.31	4.38
IT-FANG-1	Foliated biotite granite	19.9	6.5	3.60	3.38
IT-FANG-4	Biotite granite	32.4	8.9	3.67	4.87
Average					3.75

Sample numbers and analysis are from Kawada et al. (1987)

Heat production (A, μW m^{-3}) calculation uses the formula from Jaupart et al. (2016): $A = 0.257[U] + 0.069[Th] + 0.094[K]$, where U and Th are in ppm, and K is in % by weight

the sediments (discussed below). The most uncertainty in these estimates is contribution from the lower crust and heat flow from the top of the asthenosphere. Also uncertain are transient effects on asthenosphere heat flow from lithosphere thinning related to the late Oligocene–Pliocene extension of the Fang basin (e.g. Morley et al. 2011).

For the deeper sections of the five temperature-profiled wells in basin sediments (Figs. 2, 3, 8), Thienprasert and Raksaskulwong (1984) calculated heat flow values 94–150 mW m^{-2} (mean value of 114 ± 23, $n = 5$), using measured core conductivities of 1.19–1.70 W m^{-1} °C^{-1}. For the deeper sections of the two wells profiled in the sediments by Barr et al. (1979), heat flow values of 93 and 168 mW m^{-2} were calculated using an assumed conductivity of 1.26 W m^{-1} °C^{-1}. These values are higher than those from estimates of lithospheric parameters (Table 4) and much higher than 39 or 56 mW m^{-2} calculated from the temperature gradient of the 1200-m-deep well (32.8 °C/km) using either a conductivity of 1.19 or 1.70 W m^{-1} °C^{-1}. Thus there is some uncertainty on the regional heat flow, but values in excess of 90 mW m^{-2} are reasonable. If we use the lower values of measured heat flow (~ 94 mW m^{-2}), and estimate the crystalline rock conductivity of 3.0 W m^{-1} °C^{-1}, the calculated temperature gradient in the crystalline rock is 31 °C/km. From this we estimate a maximum depth to which 130 °C water circulates in crystalline rock at ~ 3 km, but allow that higher heat flow would indicate shallower depths.

Methods

The 40-year history of investigations of the Fang geothermal area have not been compiled into an integrated review since the 1980s. We document temperature and flows from seeps and wells, and established their location in UTM (Universal Transverse Mercator, WGS84 datum) coordinates. Waters from selected seeps and wells were analyzed for chemistry and geothermometry. Geology of the area was re-mapped and re-interpreted with emphasis on structure as a guide to locating the permeable fracture system. MT and DC resistivity surveys of Amatyakul et al. (2016) and Coothungkul and Chinapongsanond (1985) were reviewed for understanding structural geology and the geothermal system. We attempt to understand the permeable fracture system as a fault damage zone in the crystalline rocks related to the active Mae Chan fault. This review does not precisely locate the important fractures, but we establish a conceptual model and make recommendations on geophysical surveys that may be useful in siting new wells. We further make recommendations on potential drill sites based on existing data,

Table 3 Estimates of surface heat flow at Fang

	Thickness (km)	Heat production (low) (μW m^{-3})	Heat production (high) (μW m^{-3})	Heat production (average) (μW m^{-3})	Heat flow contribution (low) (mWm^{-2})	Heat flow contribution (high) (mWm^{-2})	Heat flow contribution (average) (mWm^{-2})	References
Upper crust (Fang)	10[a]	3.38	4.87	3.75	33.8	48.7	37.5	(1)
Lower crust	25[b]	0.10	1.30	0.68	2.5	32.5	17.0	(2)
Mantle lithosphere	90	0.00	0.02	0.01	0.0	1.4	0.9	(3)
Top of asthenosphere					12.0	27.0	20.0	(3)
Total estimated surface heat flow (mW m^{-2})					48.3	109.6	75.4	

References: (1) Kawada et al. (1987) and Table 3; (2) Jaupart et al. (2016); (3) Waples (2001)

[a] Upper crust thickness of 10 km based on an estimate of 5–10 km for typical thickness of large granitic batholiths by Petford et al. (2000)

[b] Lower crust thickness based upon total crustal thickness of 35 km determined by Noisagool et al. (2014)

Table 4 Chemistry of waters sampled at Fang Hot Springs

CODE	Sample date	pH	Temp °C	Cond. µS cm^{-1}	TDS mg l^{-1}	CO_3 mg L^{-1}	HCO_3 mg l^{-1}	Cl mg l^{-1}	SO_4 mg l^{-1}	F mg l	H_2S mg l^{-1}	NO_3 mg l^{-1}	SiO_2 mg l^{-1}
CM 3-C	1987	9.45	96		513			27.5	44	21.5			180
FANG-1	1987	9	99		510			18	23				176
Well FTGE-3	1987	8.9	98.5		499			17	19				169
Well FTGE-5	1987		99		519			18.4					180
F MINE	1987		40		342			3.63	97				50.6
Well FX-2	9-5-2011	9.17		550	440		100	9.2	16	20		< 1.0	170
Well FTGE-15	9-5-2011		130.4				110	8.8	22	19		< 1.0	170
well FTGE-14	9-5-2011	9.25		550	440		91	8.9	17	20		< 1.0	170
CM-03-8 well FTGE-14	2-2014	8.95	98.0	507	436	60.0	185.5	15.2	8.8	17.5	20	< 0.02	121.6
CM-03-2 east seep	2-2014		79.1	501	431	0.0	282.5	19	21.5	15.5	0.3	< 0.02	102.7
CM-03-3 main seep	2-2014	9.20	88.5	896	513	48.0	190.5	13.3	16.2	20.5	13	< 0.02	121.9
CM-03-4 main seep	2-2014	8.50	96.7	501	413	6.0	265.5	11.4	13.2	21.8	14	< 0.02	113.3
CM-03-5 main seep	2-2014	9.02	98.3	513	435	78.0	150.5	7.6	18.0	19.5	15	< 0.02	123.6
CM-03-6 main seep	2-2014	8.95	97.5	503	428	42.0	220.5	5.7	15.6	19.5	0.3	< 0.02	119.9
CM-03-7 main seep	2-2014	9.98	81.8	512	431	24.0	210.5	26.6	38.6	18.5	0.2	< 0.02	123.1
CM-03-9 generator outflow	2-2014	8.87	71.0	495	404	60.0	180.5	20.9	6.7	10.5	8.5	< 0.02	117.6
CM-03-10 cooling pond	2-2014	7.26	37.0	127	83	0.0	61.0	7.6	6.6	1.8	< 0.2	< 0.02	27.3
CM-03-1 north pond	2-2014	8.22	59.1	493	397	0.0	290.5	20.9	23.5	9.5	0.5	< 0.02	114.1

CODE	Sample date	NH_4 mg l^{-1}	Na mg l^{-1}	K mg l^{-1}	Li mg l^{-1}	Ca mg l^{-1}	Mg mg l^{-1}	Fe mg l^{-1}	Mn mg l^{-1}	Zn mg l^{-1}	Cu mg l^{-1}	Cd mg l^{-1}	Pb mg l^{-1}	Al µg l^{-1}	As µg l^{-1}
CM 3-C	1987		128	9.1		1.5	0.04	0.1							
FANG-1	1987		120	8.7		1.4	0.05	0.277							
Well FTGE-3	1987		120	8.8		1.9	0.1	0.35							
Well FTGE-5	1987		126	9		1.2	0.07	0.038							
F MINE	1987		54.3	8.6		28	13.6	0.25							

Table 4 continued

CODE	Sample date	NH_4 mg l^{-1}	Na mg l^{-1}	K mg l^{-1}	Li mg l^{-1}	Ca mg l^{-1}	Mg mg l^{-1}	Fe mg l^{-1}	Mn mg l^{-1}	Zn mg l^{-1}	Cu mg l^{-1}	Cd mg l^{-1}	Pb mg l^{-1}	Al µg l^{-1}	As µg l^{-1}
Well FX-2	9-5-2011	0.10	120	8.4	0.49	1.1	< 0.5	0.14	< 0.005	0.23	< 0.05	< 0.001	< 0.050	320	< 50
Well FTGE-15	9-5-2011	0.13	120	8.6	0.48	1.7	< 0.5	0.26	0.015	7.00	< 0.05	< 0.001	< 0.01	550	< 50
well FTGE-14	9-5-2011	0.09	110	8.2	0.48	1.5	< 0.5	0.34	< 0.005	0.31	< 0.05	< 0.001		280	< 50
CM-03-8 well FTGE-14	2-2014		137.7	7.8	0.53	2.3	0.002	< 0.005	< 0.005	< 0.005	< 0.005	< 0.002	< 0.005	233.0	< 5.0
CM-03-2 east seep	2-2014		136.9	7.9	0.54	5.4	0.041	< 0.005	< 0.005	< 0.005	< 0.005	< 0.002	< 0.005	164.4	10.4
CM-03-3 main seep	2-2014		140.7	8.1	0.52	2.0	0.012	< 0.005	< 0.005	< 0.005	< 0.005	< 0.002	< 0.005	173.1	< 5.0
CM-03-4 main seep	2-2014		136.4	8.1	0.51	3.1	0.004	< 0.005	< 0.005	< 0.005	< 0.005	< 0.002	< 0.005	98.7	< 5.0
CM-03-5 main seep	2-2014		138.5	7.6	0.55	1.8	0.028	< 0.005	< 0.005	< 0.005	< 0.005	< 0.002	< 0.005	184.3	7.3
CM-03-6 main seep	2-2014		137.1	8.1	0.51	3.0	0.005	< 0.005	< 0.005	< 0.005	< 0.005	< 0.002	< 0.005	179.8	< 5.0
CM-03-7 main seep	2-2014		140.0	9.4	0.54	2.4	0.005	< 0.005	< 0.005	< 0.005	< 0.005	< 0.002	< 0.005	228.5	< 5.0
CM-03-9 generator outflow	2-2014		136.2	8.1	0.52	2.3	0.002	< 0.005	< 0.005	< 0.005	< 0.005	< 0.002	< 0.005	225.6	< 5.0
CM-03-10 cooling pond	2-2014		30.1	3.0	0.06	8.9	1.223	< 0.005	< 0.005	< 0.005	< 0.005	< 0.002	< 0.005	27.2	12.4
CM-03-1 north pond	2-2014		133.7	9.1	0.53	6.1	0.076	< 0.005	< 0.005	< 0.005	< 0.005	< 0.002	< 0.005	35.9	6.3

Table 4 continued

CODE	Sample date	Alkalinity mg l^{-1} $CaCO_3$	Hardness mg l^{-1} $CaCO_3$	%error Cat An^{-1} balance	Source
CM 3-C	1987	237			1[a]
FANG-1	1987	245			1[a]
Well FTGE-3	1987	247			1[a]
well FTGE-5	1987	255			1[a]
F MINE	1987				1[a]
Well FX-2	9-5-2011				2[b]
Well FTGE-15	9-5-2011				2[b]
Well FTGE-14	9-5-2011				2[b]
CM-03-8 well FTGE-14	2-2014	272	25.8	− 1.6	3[c]
CM-03-2 east seep	2-2014	232	31.2	− 3.2	3[c]
CM-03-3 main seep	2-2014	252	29.9	− 3.6	3[c]
CM-03-4 main seep	2-2014	230	24.7	− 3.2	3[c]
CM-03-5 main seep	2-2014	279	31.7	− 1.8	3[c]
CM-03-6 main seep	2-2014	265	29.7	− 2.3	3[c]
CM-03-7 main seep	2-2014	221	31.5	− 1.9	3[c]
CM-03-9 generator outflow	2-2014	268	25.4	− 3.7	3[c]
CM-03-10 cooling pond	2-2014	50	3.4	− 0.5	3[c]
CM-03-1 north pond	2-2014	238	30.5	− 3.0	3[c]

[1] Hirukawa et al. (1987)

[2] Lara Owens, Ormat Corp. written communication

[3] This study: analysis by the Office of Primary Industries and Mines, Region 3, Chiang Mai, using ICP, except F and Cl by ion selective electrode

data that should be taken during drilling, the importance of production-well diameters sufficient for pump settings, and the importance of re-injection wells.

Geologic mapping at the geothermal area

Geologic framework

The hot springs lie about 1 km north of the NE–SW-trending Mae Chan fault, the obvious large structure with physiographic expression (Figs. 4, 6, 9). The fault trace is expressed as edges of hilly topography and as aligned saddles along ridges in the hills (Fig. 6). The fault forms a steeply dipping contact (based on MT data) of the Paleozoic sedimentary rocks with Cenozoic alluvial fan deposits and the underlying coarse-clastic sediments of the Mae Fang Formation. Contact of the Paleozoic sedimentary rocks with the foliated granite and mylonite (presumably of Triassic age) also trends NE–SW similar to the Mae Chan fault, however, the v-shape contact pattern indicates a shallow SE dip showing that the contact is a low-angle normal fault, or a detachment fault (Figs. 9, 10). The Mae Chan fault trace has right-stepping segments at its western end (Fig. 4).

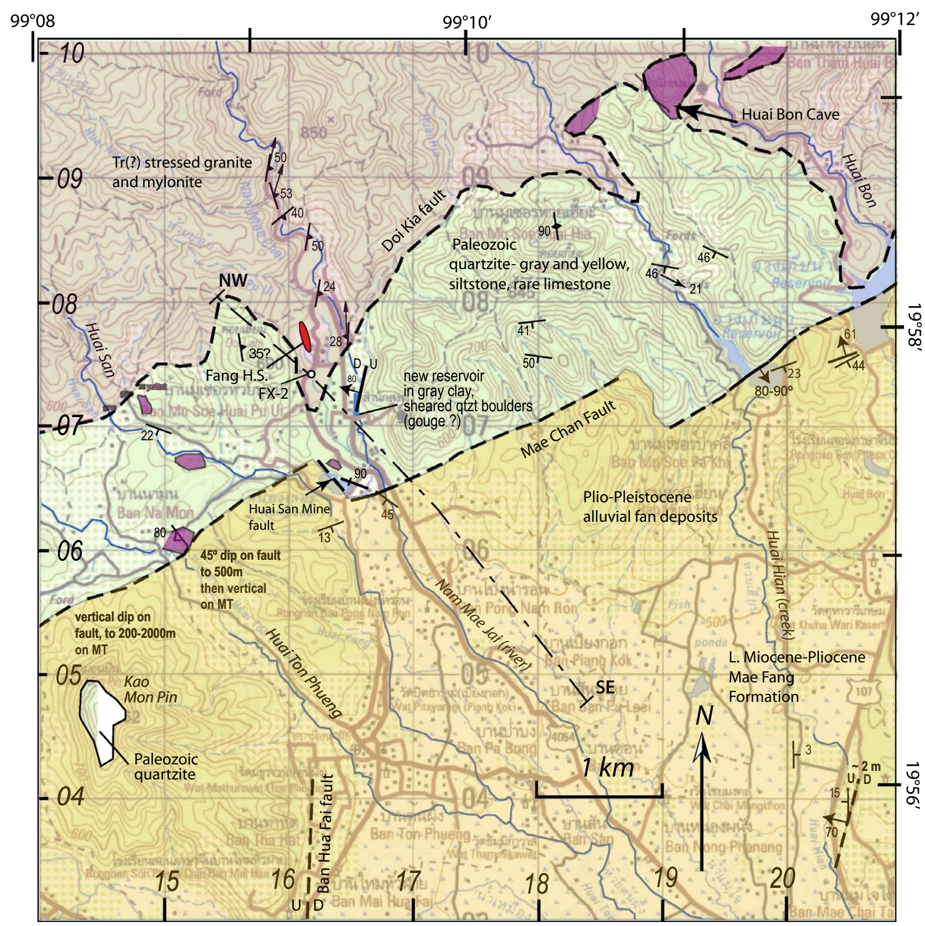

Fig. 9 Geologic map of the Fang geothermal area based on mapping by the authors (2014–15) and by Chiang Mai University (Ensol Co., Ltd. 2015). The irregular contact of Paleozoic sedimentary rock with crystalline rocks is interpreted as a low-angle normal fault, called the Doi Kia fault. FX-2 is the geothermal well south of the hot springs. Limestone outcrops in purple color. Coordinates are UTM, WGS-84

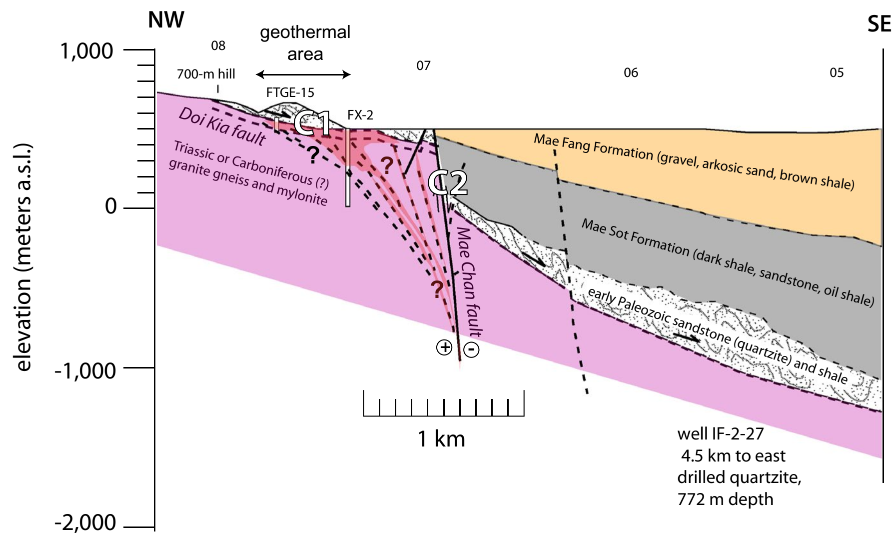

Fig. 10 NW–SE Cross section of the Fang geothermal area—location of section shown in Fig. 9. FTGE-15 and FX-2 are producing geothermal wells. C1 and C2 are MT anomalies discussed in text

Lithology found in the early geothermal drilling was mostly granitic and cataclastic rocks; however, wells FTGE-2, BH-3, and BH-5 drilled into quartzite (Ratanasthien et al. 1985, p. 19). We have been unable to obtain records of lithology for wells drilled since 1982 (wells since FTGE-5). The cataclastic nature of the foliated granite and gneiss is confirmed by Chiang Mai University geologists (Ensol Co., Ltd. 2015) who mapped much of the exposed rock as mylonitic gneiss and schist. We have tried to reconcile these lithologies with the regional stratigraphy shown by Imsamut and Krawchan (2005) (Fig. 11).

Paleozoic sediments

A band of Paleozoic sedimentary rocks forms the hills between the crystalline rocks of the high mountains, and the rolling foothills underlain by Cenozoic sediment (Figs. 2, 3, 9). Contact with the crystalline rocks is a low-angle (15°) normal fault. Contact with the Cenozoic sediments is a high-angle strike-slip Mae Chan fault. The sediments observed in outcrop are mostly thick-bedded quartz sandstone with interbeds of shale, and massive limestone: lithologies similar to the descriptions by Imsamut and Krawchan (2005) for the lower 1000 m of strata (Ordovician–Silurian Hod Formation) of their composite section (Fig. 11).

Quartz sandstone

Much of the Paleozoic sedimentary rock is thick-bedded quartz sandstone and quartzite, in which bedding is rarely observed. This rock covers most slopes as abundant fragments, but ledges with indistinct bedding occur in places. The sandstone is composed of interlocking quartz grains, 0.3–0.6 mm, well sorted, but without observable porosity (Fig. 12a). The Paleozoic quartzite is described in thin section by Ensol Co., Ltd. (2015) as a quartz arenite with subround grains less than 0.6 mm. In outcrop the sandstone is yellowish in color, and the fresh rock is gray. In many places, the sandstone is laced with white quartz veinlets. Folded shale and thin-bedded sandstone are exposed in road cuts

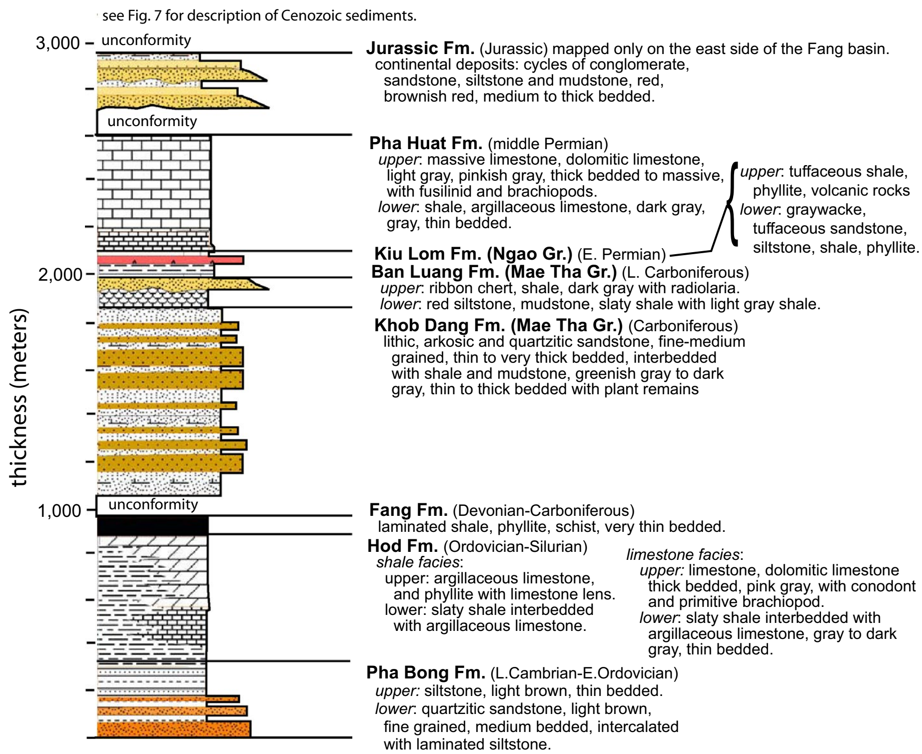

Fig. 11 Stratigraphic column of Paleozoic rocks from Imsamut and Krawchan (2005) based on their mapping of the Amphoe Fang (4848 IV) and Doi Pha Wok (4748 I) map sheets

in the Huai Hian valley (Fig. 12b, c). Faulted quartz sandstone crops out on the east bank of the Mae Chai River (Fig. 12d). West of the Mae Chai River (on Doi Liam) sandstone lies directly upon crystalline rocks. In the bed of the Mae Chai River, south of the hot springs (0516700E, 2206650N), the base of the sandstone unit is a black quartzite breccia, and similar black breccia also occurs near the contact with crystalline rocks in Huai Hian.

The lithology of this quartz sandstone, siltstone, and shale unit best matches the description of the Late Cambrian Pha Bong Formation (Fig. 11); however, thick-bedded sandstones in the Carboniferous Mae Tha Group are of similar lithology (Imsamut and Krawchan 2005). Because of poor exposure and lack of fossils one cannot be certain of the correlation of this rock type to the Late Cambrian sandstone.

Gray limestone

Scattered large (up to 2 m in size) blocks of gray limestone occur in some areas west of the hot springs (Fig. 12e), and in the valley of Huai San (creek). Limestone outcrop areas are shown in the map (Fig. 9). Largest blocks are about 7 m, which may be the thickness of an individual bed. Shawe (1984) noted large blocks of limestone embedded in deformed shale at the Huai San Fluorite Mine. Thicker beds occur on the east side of Huai Hian near the contact with crystalline rocks. The limestone at the Huai Bon Cave is at least 50 m thick. It is recrystallized and zones of calcite-cemented breccia occur in places. At Huai Bon Cave, where the limestone rests directly upon crystalline rocks, we interpret that contact as the Doi Kia fault.

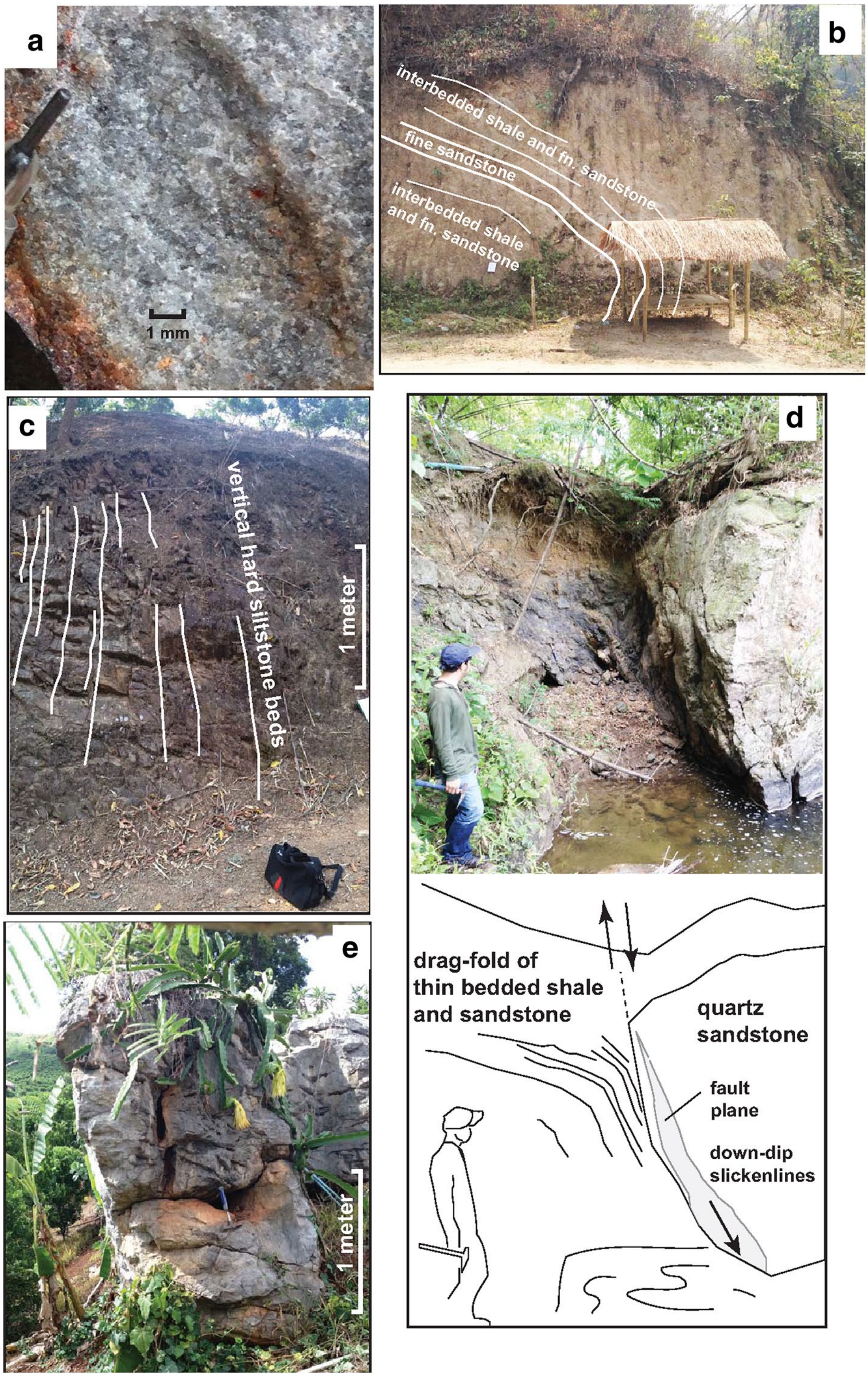

Fig. 12 **a** Close-up photo of orthoquartzite (quartz arenite) showing interlocking grains of ~ 0.6 mm. **b** Outcrop of interbedded sandstone and hard shale, fold axis plunges 21° in the 120°direction, upper limb beds dip 46° SW, and strike 102° (outcrop face oriented 068°, located at 518940E, 2208249N). **c** Outcrop of medium-bedded hard siltstone, near vertical dip, 122° strike, bedding shown by white lines (located at 518173E, 2208558N). **d** Outcrop of fault in the bed of the Nam Mae Chai River at 516585E, 2207275N), showing normal fault striking 020° dip 80°NW, with drag on the thin-bedded shale and sandstone. Photo is looking south. **e** Outcrop of gray limestone at 514850E, 2207100N

Occurrences of limestone in the Fang area are conspicuous boulder fields, ledges, and cliffs. If limestone occurs within the otherwise deeply weathered sediment, limestone always crops out. The limestone here best matches the description of the limestone facies of the upper Silurian Hod Formation (Fig. 11). These limestone occurrences should not be confused with the well exposed high cliffs and karst towers of the early Permian Ngao Group (Doi Chiang Dao limestone) which lie to the west and south of Fang Basin. We believe the limestones in the hot springs area are those of Silurian age. No macrofossils were found, as much of the limestone is recrystallized.

Dark gray claystone

Gray shale is exposed in the east wall of the water-filled pit of the Huai San fluorite mine and contains disseminated fine pyrite and black carbonaceous particles. Shawe (1984) observed large limestone blocks embedded in the deformed shale near a fault in the mine pit (Fig. 13). Dark gray shale lies directly on crystalline rocks in the draw at 0515290E, 2207500N.

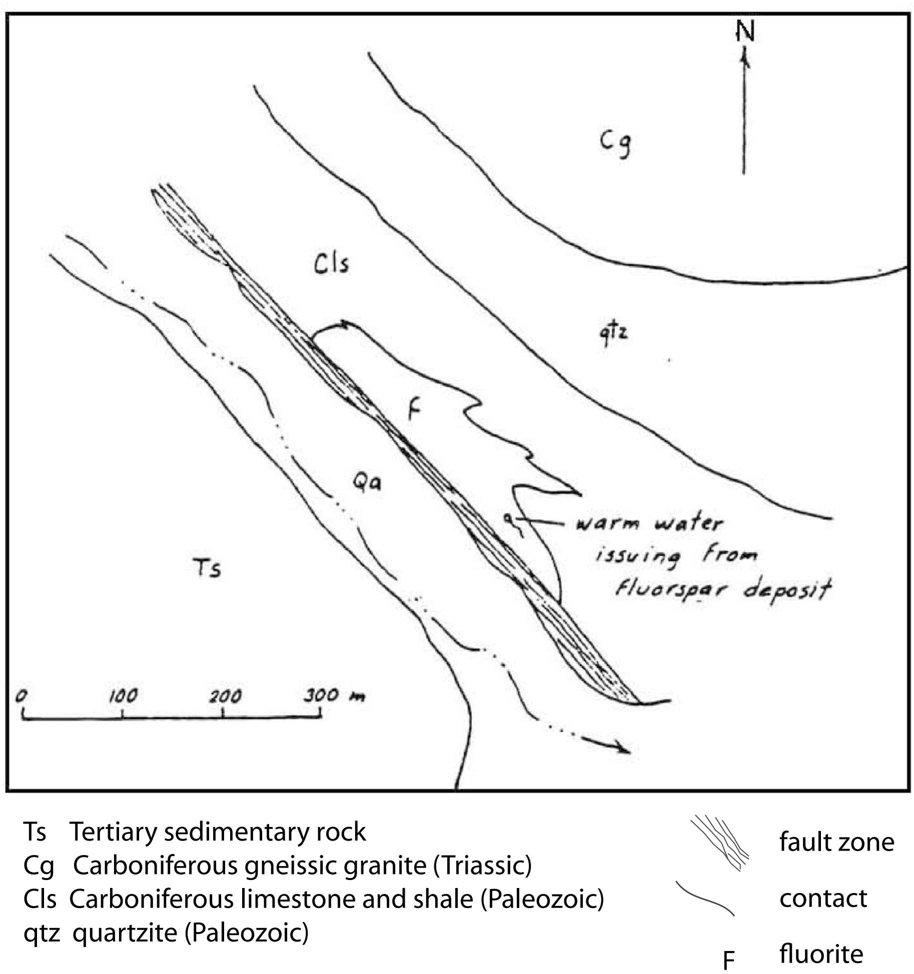

Fig. 13 Sketch map of the Huai San fluorite mine made by Shawe (1984) showing location of warm springs in the mine. Carboniferous ages assumed at the time are now considered early Paleozoic sediments and Triassic granite

Just above the contact with crystalline rocks, a 12-m-deep-reservoir was excavated in 2016 into a massive, dark gray, gummy claystone with chunks of gray sheared quartzite, with no discernible stratification (Fig. 14). In thin section, the quartzite is composed of granulated angular quartz grains less than 0.1 mm. Location of reservoir is shown in Fig. 9. We are uncertain whether this excavation is in a shale bed or in gouge of the Doi Kia fault. Observed thicknesses of shale are limited to excavation exposures which are no greater than 12 m. Hills which cover much of the area of Paleozoic sediment without outcrops may be entirely shale. These gray clayey rocks may be the shale facies of the Ordovician–Silurian Hod Formation (Fig. 11).

Crystalline rocks (Presumably of Triassic age)

Crystalline rocks in the geothermal area are a group of foliated granite, augen gneiss, minor schist, and mylonite. These foliated or "stressed" granites" yield late Permian to Triassic ages throughout northern Thailand using a variety of isotopic geochronometers (Compilation by Crow 2011). Similar gneissic basement rocks in the Inthanon Zone to the south are regarded as Sibumasu basement that has been metamorphosed during the Indosinian Orogeny of late Permian to late Triassic age (Ridd et al. 2011; Gardiner et al. 2016). No stratigraphic contacts between these "basement crystalline rocks" and Paleozoic cover have been identified (Barber et al. 2011, p. 515), and many contacts are interpreted as low-angle detachment faults.

Foliated crystalline rocks

Best exposed along the bed of the Nam Mae Chai (river), east of the hot springs, are mylonite and augen gneiss and granite gneiss (Fig. 15a, c, f). Biotite and feldspar- augen (typically 5 × 2 mm) are the visible foliation. Rarely, very elongate dark inclusions are observed. Porphyroclasts occur sparsely (Fig. 16a), but rotation directions have not been evaluated. Foliation strike observed in outcrops along the Nam Mae Chai (river) is

Fig. 14 Photograph during January, 2016 excavation of pit into dark-gray sheared quartzite, sheared pieces embedded in gray gummy clay. Resulting reservoir is ~ 12 m deep. This clayey material apparently lies within or beneath the quartzite just east of the hot springs. No bedding planes observed (clean exposure is left side of photo). No pyrite or visible mineralization observed in the clay or rock. Location is 0516550E, 2207200N

Fig. 15 Photos of gneiss and mylonite: **a** foliated granite with sheared porphyroclasts at the hydroelectric plant bridge (516237E, 2208078N) (pencil diameter is 9 mm). **b** ultra-fine-grained mylonite on the west side of Huai Hian (creek) (0518528E, 2208928N) showing foliation striking 108° and dipping 11°SW (coin diameter is 25 mm). **c** photo showing foliated (178°strike, 28° W dip) mylonite, with quartz veins showing strike-parallel lineation at bridge (516449E, 2207718N). **d** coarse grained, weakly foliated biotite granite (weathered to brown color) in cut on road to Haui Born Cave (519819E, 2209366N). **e** photo looking west at the hot springs area and steam plume from the FTGE-7 well. Hot springs area is studded with corestones of foliated granite. **f** photo showing fractures in foliated granite filled with brownish veinlets of chalcedony (?) (515300E, 2207520N)

generally N–NE, and foliation dip is 24–50°E, although some west dips occur. Lineation is near horizontal directed along N-NE strike of the foliation. Mylonite is best seen in the river bed just north of the bridge (0516500E, 2207675N) (Fig. 15c) and one outcrop of a fine mylonite on the west side of Huai Hian valley (0518528E, 2208928N) (Fig. 15b).

Slightly foliated coarse-crystalline biotite granite

Coarse-crystalline biotite granite was mapped by Imsamut and Krawchan (2005) in the hot springs area, and to the east, however we noted that all the crystalline rocks are somewhat foliated. Along the road to Huai Born Cave, the granite is coarse crystalline and less foliated than elsewhere, and this may be the lithology that they noted (Fig. 15d).

Hydrothermally altered crystalline rock

The cuttings from FTGE-7 (53 m total depth) were sampled, and the clay minerals of 3 zones, determined by X-ray diffraction analysis (Ratanasthien et al. 1985, p. 94–96). At 5.25 m the dominant clay is montmorillonite with other minerals, quartz, illite, and feldspar present. Below this is a zone with montmorillonite-mordenite. The upper montmorillonite–mordenite zone is generally beneath boulders of foliated granite in the area of hot spring manifestation (Fig. 15e). Below that zone at 23.5 m depth the dominant clay-mica mineral is chlorite associated with illite, quartz, feldspars, and calcite. Unfortunately, quantitative data are not available nor is mineralogical examination reported for the other wells. Boulders of foliated granite in the hot springs area do not appear altered, perhaps because they are resistant core stones within the clay-altered granite.

Cenozoic basin sediments

Maximum basin fill is 2800–3000 m. The beginning of basin formation is late Oligocene, in common with other extensional basins in Northern and Central Thailand (Morley et al. 2011).

Mae Sot Formation, lower Miocene

The early basin fill rocks (Mae Sot Formation) crop out within the basin south of Fang, and extensively on the southeast margin of the basin (Imsamut and Krawchan 2005). No outcrop areas are shown along the northwest margin near the hot springs. Stratigraphy of Mae Sot Formation is known from petroleum exploration wells (Fig. 7). Overlying the pre-Cenozoic bedrock is > 500 m of fluvial sandstone and lacustrine claystone of the Mae Sot Formation, the top of which contains up to 22 m of coal. The overlying sequence of the formation is lacustrine coal and oil shale, > 700 m thick. Age is early-mid-Miocene. Within the Mae Sot Formation is a local angular unconformity associated with an uplift of the eastern margin of the basin, probably marking an inversion event in the Middle Miocene (Morley and Racey 2011).

Mae Fang Formation, upper Miocene–Pliocene

Unconformably overlying the Mae Sot Formation is a > 700-m-thick unit of coarse arkosic sandstone with minor interbedded shale and sandy conglomerate, some containing coalified wood (Fig. 16a), designated the Mae Fang Formation. Exposures of these sediments that have been deformed by faulting or moderate folding (Fig. 16) are regarded as Mae Fang Formation, whereas gravels with moderate dip or horizontal are believed to be the overlying alluvial fan unit. The Mae Fang Formation (map unit labeled "N", in Figs. 2, 3) occurs as rolling hills out in the middle of the basin, north of Fang, hills that rise to 500 m elevation above the surrounding 460 m elevation floodplain. We observed an excavation exposure of the unit along Highway 107 (0520446E, 2203790N), where the unit is composed of gravelly angular sand and clayey sand, with irregular scour-fill boundaries. The layers dip 15°W, strike 000°, and are cut by a 70° NW, 015° strike, with apparent high-angle reverse, up to east displacement of about 2 m (Fig. 9). Some of the

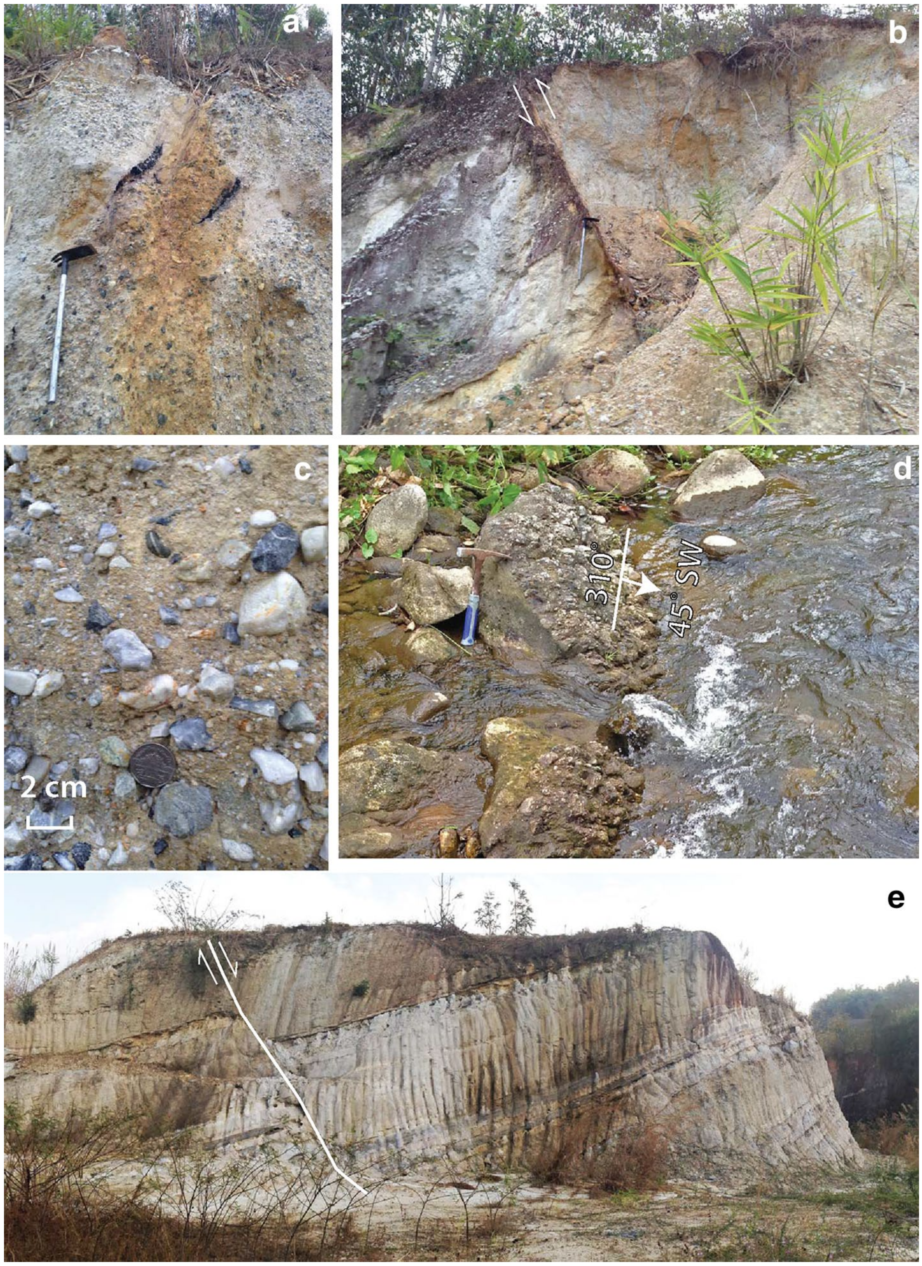

Fig. 16 Photos of Cenozoic Mae Fang Formation sediment. Photos (**a**–**c**) are located 100 m west of the national park check station on the road to Doi Pha Hom Pok at (520495E, 2207547N). **a** Clayey, sandy gravel with lenses of coalified wood dipping 44°SE. **b** Reverse fault (strike of 070°, dip of 61°NW) in sandy gravel. Footwall sediments dip 44°SE. Digging hoe, 1 m long, for scale. **c** Close-up photo of sandy gravel of photo (**a**). Clasts are entirely dark gray to white quartzite with white quartz veinlets. **d** Sandstone and conglomerate (strike 310°, dip 45°SW in the bed of the Nam Mae Chai (river), on the immediate SE side of the Mae Chan fault (516790E, 2206410N)). **e** Normal fault (strike 025°, dip 39°NW, 2 m offset) in pebbly sandstone of the Mae Fang Formation striking 001° to 335°, and dipping 25° to 34°. Base of section (lower right) is 2 m of gray silt with coalified plant detritus. Excavation is 11 m high. Location is 700 m west of Ban Hua Na School at (513584E, 2203193N)

areas mapped as "Quaternary terrace deposits" by Imsamut and Krawchan (2005) are faulted and moderately dipping, so that we regard most of the rolling hills as Mae Fang Formation. Imsamut and Krawchan (2005) map three different units of late Tertiary and

Quaternary age: the alluvial fan unit (Qaf), the terrace unit (Qt), and the colluvial unit (Qc). We are uncertain of the mapping of the undeformed Quaternary alluvial fan and terrace deposits, for they cannot be distinguished from one another by lithology or clast content.

The Mae Fang Formation is interpreted as having been deposited in braided river and alluvial fan environments. Inversion anticlines along the east-dipping boundary fault have eroded crests and are unconformably overlain by deposits of Quaternary gravels, sand, and clay, locally at least 100 m thick (Morley and Racey 2011).

Coarse alluvium of the Mae Fang Formation indicates that alluvial river systems flowed through the Fang basin, over the previously deposited swampy deposits of the Mae Sot Formation. Outlet of the basin was presumably controlled by downcutting of the Kok River and its capture of the Fang drainage basin. Confluence where the Fang River now flows into the Kok River is now 444 m elevation. Gorge of the Kok River on its course to Chiang Rai cuts through hills rising to 800 m elevation above the ~ 430-m elevation channel; therefore the river has incised about 370 m, during which time coarse alluvium accumulated in the basin.

Undeformed alluvial fan and colluvial deposits

Alluvial fan and colluvial deposits are mapped separately along the west side of Fang basin by Imsamut and Krawchan (2005). We see no mappable difference between these two units. Where exposed, both are comprised of thick-bedded, boulder alluvium with several thick beds of moderately well-sorted sand. The unit mapped as the alluvial fan deposits is well exposed on an 18-m-high quarry face, over a distance of 120 m at (0516371 E, 2204641N) on the north side of Huai Ton Pheung (Fig. 17). The deposit is mostly sandy, subround, cobble-and-boulder gravel. A conspicuous white, coarse, sand

Fig. 17 Horizontal clayey, sandy gravel of the Mae Taeng Formation. Subround clasts are entirely quartzitic sandstone with veinlets of quartz up to 40 cm diameter. Quarry wall is ~60 m high, comprised of a lower 4 m of clayey sandy boulder gravel, 1.5 m of sand, 4 m of fining upward sandy boulder gravel with a sandy top, and 8 m of clayey boulder gravel. Upper 40 m poorly exposed clayey, sandy gravel. Location is along the Huai Ton Pheung Road, 0.5 km NW of Ban Ton Pheung, (516322E, 2204677N)

bed 1.5 m thick, fining upward to a 0.5 m dark gray-red mottled clay lies within the gravel. Clasts here are predominantly sandstone. No gneissic or granitic clasts occur, and lithology is similar to the underlying Mae Tang Formation. Deposits of subround boulder gravel, grain-supported in a red sandy clay matrix occur in hills to south, observed at elevation 620 m, and apparently much higher on the flanks of Kao Mon Pin, up to about 800 m elevation (Fig. 9). At the very top of Kao Mon Pin, elevation 862 m, Imsamut and Krawchan (2005) show an outcrop of Carboniferous sandstone (Khop Dong Formation) (22014600E, 0504700N). Coarse, bouldery alluvial fan sediment apparently filled around the earlier hilly topography of Paleozoic rock up to ~ 800 m elevation. Similarly, at hill "750 m" near Ban Mai Hua Na, south of the Mae Nam Mao (22013100E, 0501650N) is bouldery sediment up to 700 m elevation. The main flood plain of the Fang River is now at 460 m elevation, beneath which are 700 + m of coarse alluvium of the Mae Fang Formation. Hills of the same coarse alluvium form these outcrop areas which rise 240 to 340 m above the plain to 800 m elevation, on the west side of the western boundary fault indicating up to 1040 m of Mae Fang Formation fill the basin.

These elevations have implications for incision of basin by the Fang River, tributary to the Kok River. In order to provide gradient for deposition of coarse gravel, the base level of the Kok-Fang River confluence junction must have been below 800 m, perhaps 650 m. The confluence of these rivers at Thaton is now 460 m elevation suggesting incision of Fang basin sediment of at least 200 m.

Virtual lack of gneissic or granitic clasts in any of the gravel outcrops (except those in the modern stream deposits) indicates that the crystalline rocks have only recently been exposed to drainages feeding the northern Fang basin.

Geophysical surveys

DC resistivity surveys-1985

Several DC electrical resistivity surveys, both Schlumberger soundings and transverse profiling, have been run over the area, but the only geophysical reports available to us are Ramingwong et al. (1980), Ratanasthien et al. (1985,) and Coothungkul and Chinapongsanond (1985). Ramingwong et al. (1980) made Schlumberger soundings at 50 points spaced 0.7 to 2 km over a 30 km^2 area between Huai Ton Phueng on the west, and Huai Bon on the east. For $AB/2 = 250$ m, they found low values (< 50 Ωm) over a 1.5 km^2 area about the hot springs (AB is the separation distance of the current electrodes, and $AB/2$ indicates the approximate depth of investigation). Coothungkul and Chinapongsanond (1985) made Schlumberger soundings at 20 locations (Fig. 18) and the apparent resistivity curves of these soundings are shown in Fig. 19. On six of the soundings they show low apparent resistivity (5–12 Ωm) at depths of 2–50 m (Fig. 19). The soundings values are contoured on 5 maps in their report for $AB/2 = 5$, 25, 50, 80, 100 m. We show their $AB/2 = 100$ m map in Fig. 18. The < 60-Ωm contour contains many of the hot wells. This EW to NE trending pattern of low resistivity is on all five maps.

Coothungkul and Chinapongsanond (1985) ran six lines of lateral resistivity profiling, using a fixed separation of current and potential electrodes, and an electrode spacing of 20 m, except Line H-1 which was 10 m. Lines H-2, H-3, and H-4 (not shown) are outside the area of hot springs (Fig. 18) and generally have high values (60 to > 200 Ωm). H-2 shows a low of 42 Ωm at station 320 and rises sharply to > 200 Ωm to the east on the

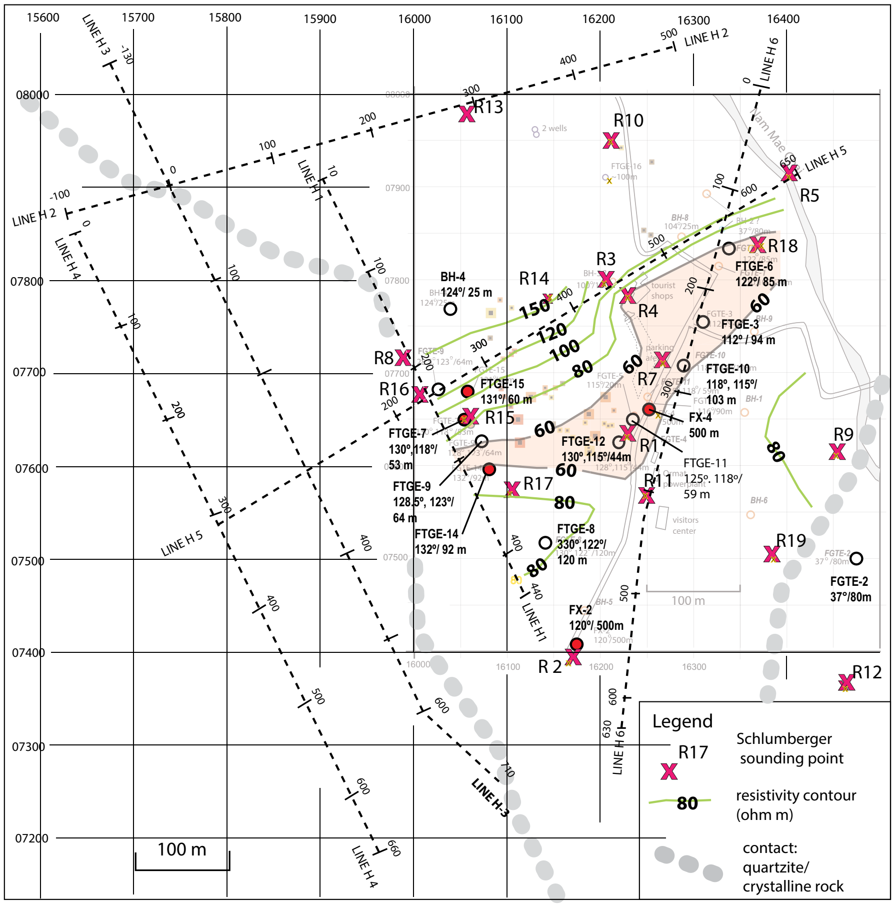

Fig. 18 Map showing Schlumberger sounding points of Fig. 19, locations of lateral DC resistivity profiles H1, H5, H6 (shown on Fig. 20), and contoured anomalously low apparent resistivity ($AB/2 = 100$ m) areas from Coothungkul and Chinapongsanond (1985)

$AB/2 = 50$ m electrode spacing. H-3 shows a low value of 52 Ωm at stations 280–300. H-4 show high values > 200 Ωm, except for low values to 85 Ωm centered at station 280 and then abruptly lower (~ 60 Ωm) east of station 490.

Lines H-1, H-5, and H-6 run through the hot springs area (Fig. 18). Line H-1 shows low resistivity (20–30 Ωm) between stations 195–290 on the $AB/2 = 50$ m profile about 20 Ωm lower than that on the $AB/2 = 100$ m profile (Fig. 20). These low resistivities are along the line of hot wells, FTGE-9, -7, and -14. It is significant that at the south end of line H-1, station 420 exhibits low resistivities of 30 Ωm on the $AB/2 = 50$ profile. That area to the south contains hot well FTGE-8 and producing well FX-2. Line H-5 shows mostly moderate resistivities > 40 Ωm, except for low values of 15–25 Ωm between stations 240–260. These low values also correspond to hot well FTGE-16. Line H-6 shows low values < 40 Ωm from stations 160–340, corresponding to hot wells FTGE-6, -11, and producing well FX-2. A low value is also at station 475.

Location of 7 E–W trending resistivity survey lines, spaced 100 m apart, is shown in a map in Wanakasem and Takabut (1986), but no copy of that resistivity data is available.

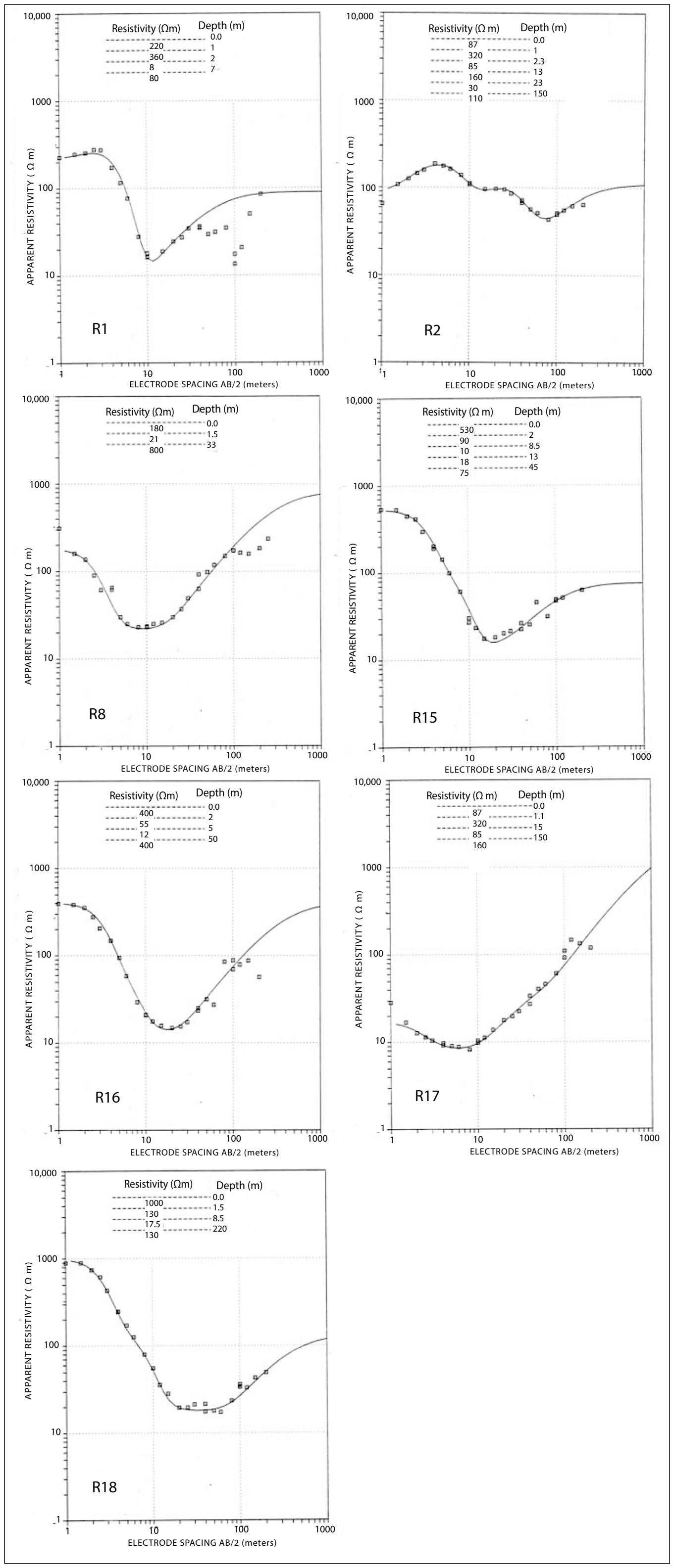

Fig. 19 Schlumberger array resistivity soundings from Coothungkul and Chinapongsanond (1985). Low apparent resistivity (< 60 Ωm) occurs in a zone 9–60 m depth on most soundings. Location of soundings shown by the X symbol in Fig. 18

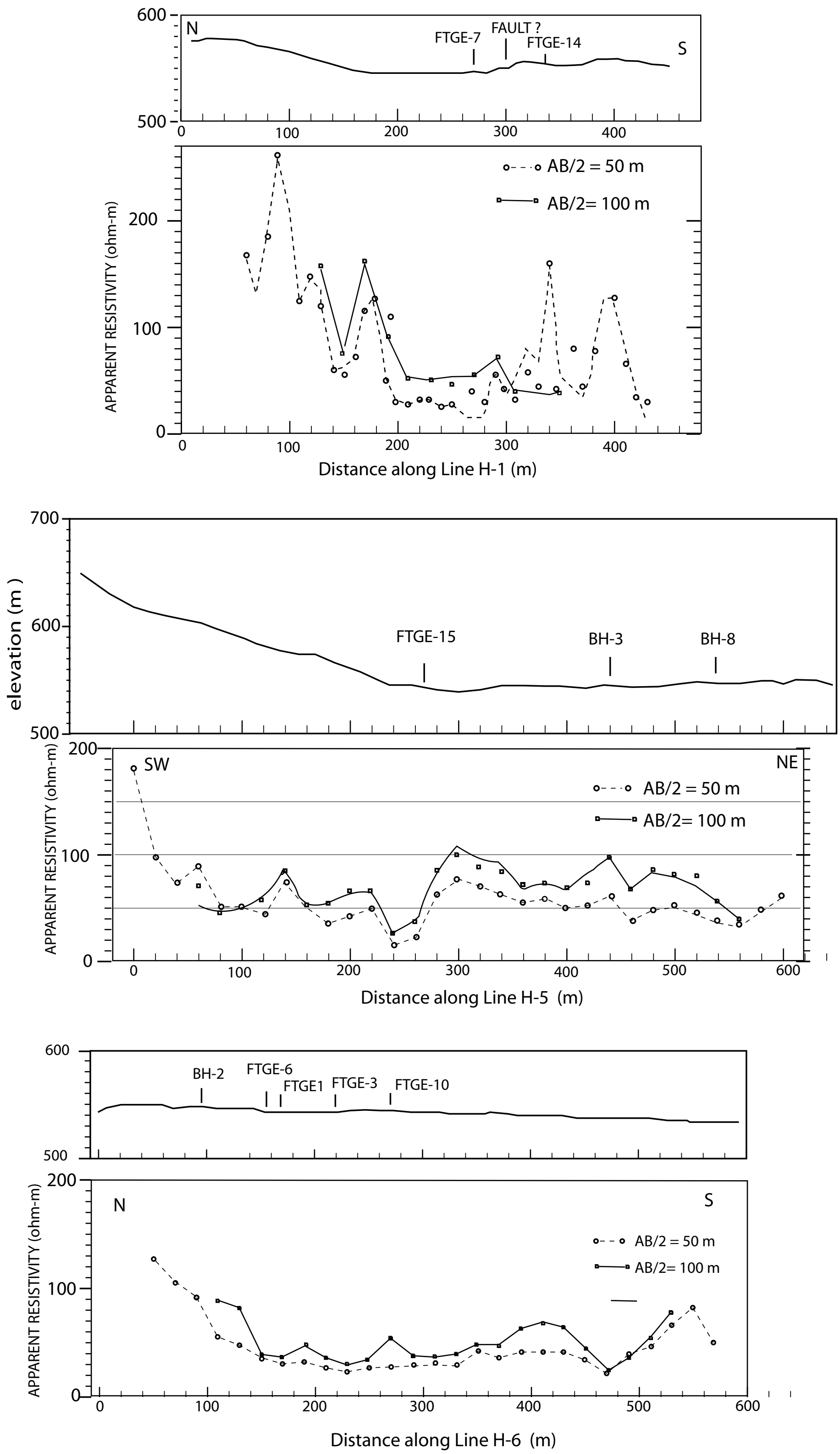

Fig. 20 DC lateral resistivity transects (Lines H1, H5, and H6) of *AB*/2 = 50 m, and *AB*/2 = 100 m, locations shown in Fig. 18 from Coothungkul and Chinapongsanond (1985)

One concludes from Coothungkul and Chinapongsanond's report that the low resistivity zone (< 45 Ωm) is shallow, 9–60 m, over the geothermal area and that the deeper rock is > 80 Ωm. Considering the relatively high resistivity of the thermal water (5.6 Ωm), they concluded that these low resistivity zones are caused by hydrothermal alteration of the crystalline rocks. Depth resolution of their surveys is unable to detect deeper fracture systems, but the precision of these lateral surveys to locate sharp boundaries indicates that dense surveys such as line H-1 with 5-m electrode spacing, and longer AB spreads, would be useful in further exploration. DC resistivity surveys can be deployed rapidly with modern equipment, and processed to produce 2D and 3D tomographies (e.g., Revil et al. 2015).

Magnetotelluric (MT) survey

MT measurements were made at 25 points spaced 250–1000 m apart over a ~ 20 km^2 area south of the hot springs by Amatyakul et al. (2016) (Fig. 21). Their paper presents MT slices at depth levels of 0, 50, 200, 400, 600, and 1000 m. We show additional levels at 25 and 300 m depths (Fig. 21) from an earlier data report by Siripunvaraporn (2015). The 3D MT inverted data (Figs. 21, 22) show the high resistivity (> 300 Ωm, colored blue) crystalline rock overlain by low resistivity (< 30 Ωm, colored yellow and orange) material. Station numbers discussed on profiles are length in meters from the NW end of profile. The profile (Fig. 22a) shows the top of the crystalline rock dipping south at about 15° beneath low resistivity material from station 500 to 1350. The geologically mapped Doi Kia fault that places Paleozoic quartzite and shale over crystalline rock dips at a similar angle along this profile (Fig. 10). At station 1350 this shallow layer appears faulted up to the SE about 100 m. This shallow (< 200 m deep) low resistivity zone from stations 500–1600, labeled C1 in Fig. 22, is not over the geothermal area, and is not believed to be a drilling target as originally suggested in Amatyakul et al. (2016). This shallow zone is interpreted by us as shaly rock of the Paleozoic sediments. Between stations 1600 and 2000, the crystalline rock interface steepens to ~ 36°, and the Paleozoic rock thickens to ~ 500 m. At station 2100 is the mapped trace of the Mae Chan fault southeast of which is the C2 anomaly in Cenozoic sediment. The Mae Chan fault appears as a vertical structure which offsets the sediment of hundreds of meters. The sloping contact (~ 36°) from 500 to 1500 m depth may indicate another structure at the west end of the Mae Chan fault related to the western boundary fault of the basin.

The profile (Fig. 22b) traverses the geothermal area from stations 400 to 900. The profile shows a nearly horizontal zone from stations 500–1600 of material < 30 Ωm, about 100 m thick. This traverse is underlain by crystalline rock, and not Paleozoic sediment. The very low resistivity zone (< 20 Ωm) from stations 400–900 is exactly over the geothermal area and is ~ 80 m thick. We are certain from geologic mapping that crystalline rock extends along this profile to station 1550 southeast of which it is covered by Paleozoic sediment, and at station 2550 faulted against Cenozoic sediment by the Mae Chan fault. Between stations 1650 and 2400, a 36° SE dipping contact similar to Fig. 21a occurs between the high resistivity crystalline rock (> 300 Ωm) and within the overlying Paleozoic sediments, shown by the contrast of material (> 40 Ωm, colored green) overlain by lower resistivity material colored yellow and orange. The zone from station 2000 to 2400 is within the stepover zone of the Mae Chan fault, and we are uncertain how the

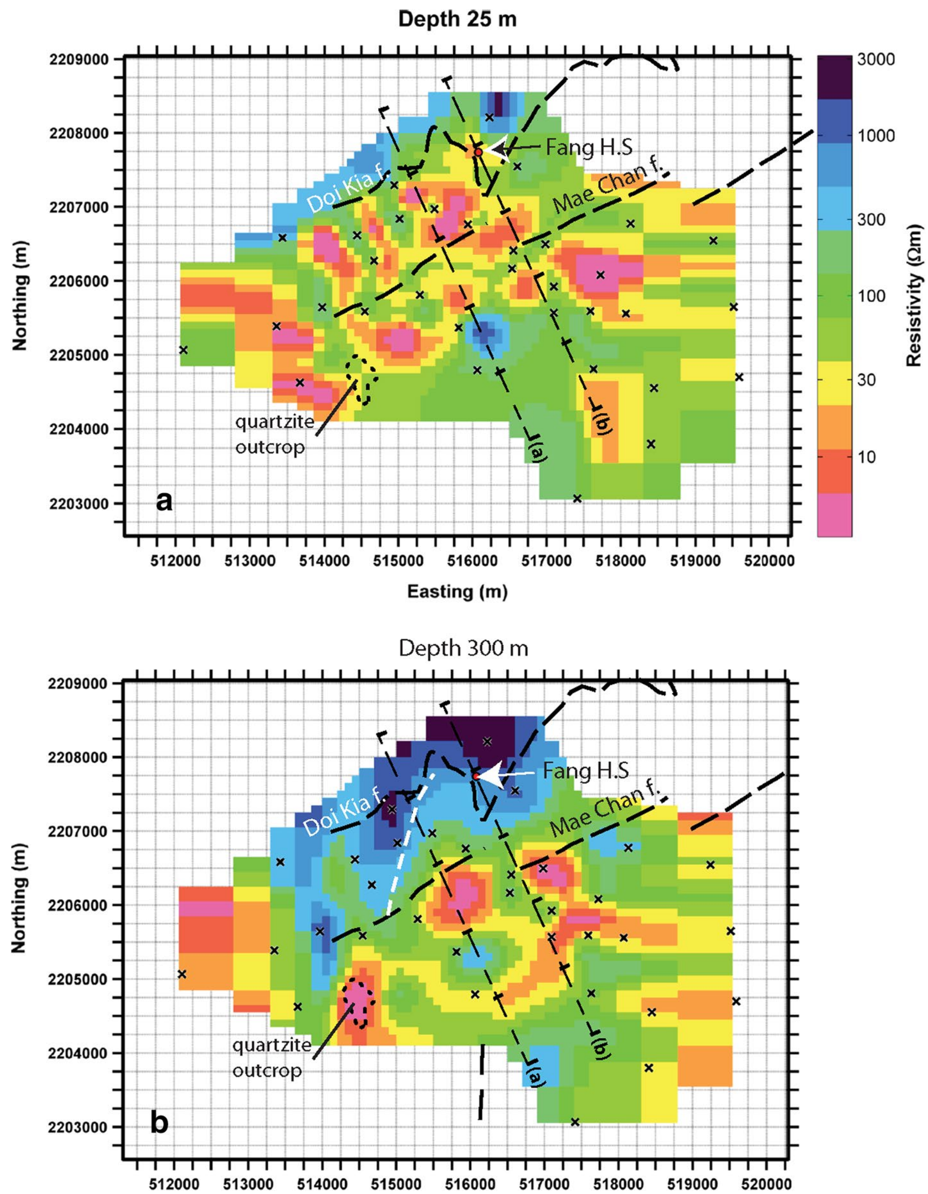

Fig. 21 Map view slices at 25 m and 300 m depths of the final inverted 3D-Magnetotelluric resistivity survey of Amatyakul et al. (2016). These slices are from an earlier report on that data by Siripunvaraporn (2015). Traces of faults from geologic mapping of Fig. 9 are dashed black lines. Map **a** (25 m depth) shows the small area of the shallow, low resistivity (< 30 Ωm, colored orange) anomaly at Fang Hot Springs. Deeper slices show only high resistivity beneath the geothermal area. The map shows low resistivity (colored orange) which is associated with the Paleozoic sedimentary rock overlying the crystalline rock (> 300 Ωm, colored blue) between the Doi Kia fault and the Mae Chan fault. Low resistivity rock south of the Mae Chan fault is the shaly Cenozoic basin fill. Map **b** (300 m) shows the crystalline rock is beneath the hot springs, and low resistivity Cenozoic basin fill southeast of the Mae Chan fault. The white line shows N–NE trending boundary between crystalline rock to the west and sedimentary rock to the east. This feature is not evident in geologic mapping, and appears only on slices deeper than 200 m. The boundary shows up clearly in cross section on the vertical slice, where it appears to dip 55°SE (Fig. 22a). The structure suggests uplifted crystalline rock to the west and may account for the isolated Paleozoic quartzite outcrop in the basin shown in the map

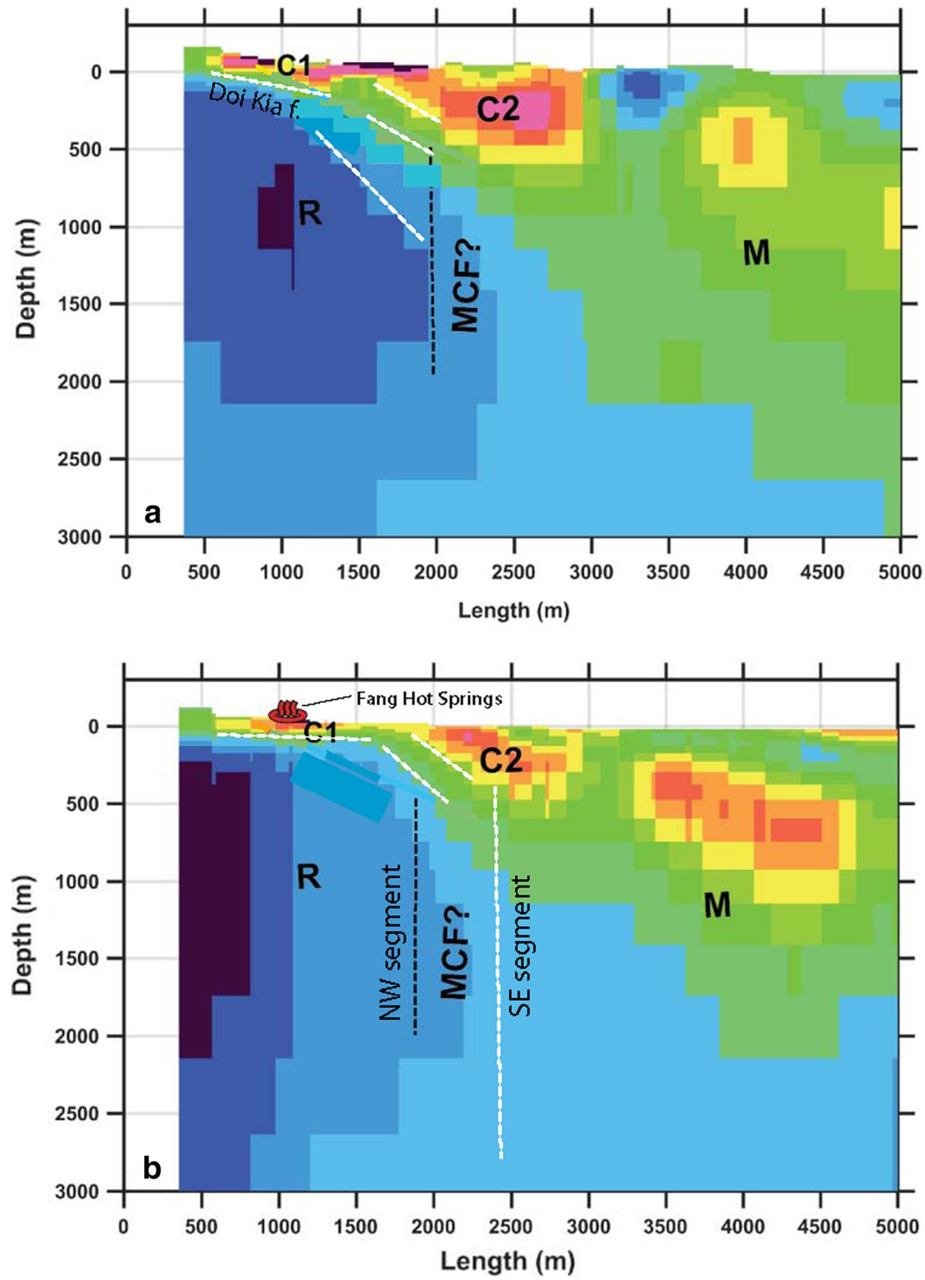

Fig. 22 Cross-sectional (vertical slices) from the 3D-magnetotelluric survey (final inverted model) of Amatyakul et al. (2016). Stations discussed in text refer to length in meters from the northwest end of profiles. Label "R" is interpreted as crystalline rock. Label "M" is interpreted as Cenozoic basin fill sediments. Profile **a** is 1 km west of the hot springs. The shallow (< 200 m) low resistivity anomaly "C1" was interpreted earlier in Amatyakul et al. (2016) as a manifestation of the hot springs. Because it lies west of the geothermal area, it is now believed to be the shaly Paleozoic sediment and perhaps the cataclastic clayey rock at the base of the Doi Kia fault. Southeast of the Mae Chan fault, the "C2" anomaly is in the shaly Cenozoic sediment. The C2 low resistivity anomaly may be caused by clay and not by hot pore water. The white line, below 400 m depth, corresponds to the N–NE trending deep structure indicated in Fig. 21b, and shows an apparent dip of 50°SE. Profile **b** is through the hot springs area and shows the flat lying, shallow (< 80 m deep) low resistivity anomaly at the geothermal area, labeled "C1." Because Profile **b** crosses only crystalline rocks from stations 1 to 1600, we believe "C1" on Profile (**b**) is caused by shallow hydrothermal alteration zones along fractures in the crystalline rocks. To the southeast, Profile **b** crosses through the stepover zone between segments of the Mae Chan fault from stations 1650–2400. The apparent 36°SE dip between those stations also occurs on profile **a** and may be a tilted structure within the stepover zone

MT imaging resolves this zone, except that crystalline rock contact (blue color) appears to dip more steeply from 500 to 1200 m depth over this distance. The line shown as the MCF is from Amatyakul et al. (2016) paper and coincides with the northern segment of the Mae Chan fault.

Because the low resistivity anomalies occur in the Paleozoic and Cenozoic sediments we interpret them as shale bodies. We have no independent information on the resistivity of Paleozoic sediments, but we mapped numerous localities of shaly rock in addition to the predominant quartzite. We know from geophysical logs that shale in the Cenozoic Mae Sot Formation typically has a resistivity of 5–10 Ωm, and is 400 or more meters thick in the southern Fang basin (Fig. 7).

The hot springs area, underlain by crystalline rocks, shows moderately low resistivity at the 25 m depth slice (< 40 Ωm) over an 150,000 m^2 area, and < 20 Ωm over a 40,000 m^2 area. This anomaly disappears at 50 m depth, and the deeper levels generally have high resistivity (100–300 Ωm). That thin layer of low resistivity material must be the hydrothermally altered crystalline rock as observed by Ratanasthien et al. (1985, p. 94–96) in the upper 23 m of well FTGE-7 and inferred from the DC resistivity surveys discussed above.

Interpretation of low resistivity in geothermal areas

In order to interpret resistivity surveys, it is important to understand the basic petrophysics of rock resistivity in geothermal areas. Needing explanation are the low resistivities (< 30 Ωm) determined by DC and MT resistivity surveys at Fang. Resistivity values of the rocks are due to electrolyte conduction in the formation water residing in the pores and fractures, and by conduction paths through clay minerals or metallic minerals. Water produced from 130 °C wells at Fang is quite low in electrolytes. The specific conductance (EC) of the water is 550 μS cm^{-1} (resistivity of 18.2 Ωm) at 25 °C. Resistivity of water decreases with temperature. The resistivity of water (R_w) occupying the pores and fractures of the 130 °C Fang geothermal reservoir has been temperature corrected with Arp's equation of Sen and Goode (1992) to 5.6 Ωm.

Resistivity of the rock due to conduction in water through the tortuous pore paths in rocks is predicted by some form of Archie's Law, and for crystalline rock it is approximately, $R_o \sim (1/\phi_p{}^m)\, R_w$, where $m \approx 2.0$ (Brace et al. 1965). Resistivity due to conduction through water in fractures generally has the form, $R_o \sim (1/\phi_f{}^m)\, R_w$, where m is 1.1–1.6 (Aguilera 1976). Porosity of pores and fractures are ϕ_p and ϕ_f, respectively. The exponent on pore porosity is ≥ 2.0, and the exponent on fracture porosity is ~ 1.0, so that fracture porosity is far more conductive because the current paths are less constricted and tortuous. If we assume a relatively large fracture porosity of 15% (i.e., a total of 15 cm of fracture openings per linear meter of rock), then the lowest calculated resistivity of such a rock mass is $R_o = (5.6\ \Omega m) \cdot (0.15)^{-1.1} = 45\ \Omega m$ (conductivity of 0.022 S m^{-1}), which does not approach the low values (< 30 Ωm) at Fang.

A fractured reservoir with hot fluid can have the same resistivity signature as clay-bearing rock, especially in the presence of the smectite clays common in hydrothermal alteration zones (Revil et al. 2015; Komori et al. 2013). Smectite has a large surface area and develops a conductive electrical double layer on its surface. Conduction on this path is called "surface conductivity" (C_s) which can greatly dominate electrolyte conductivity of water in pores (C_p) and fractures (C_f). Resistivity is the reciprocal of conductivity: $R_o = 1/C_o$. Conductivities by these paths are assumed to be parallel and are additive, so that resistivity of rock (C_o) containing clay can be approximated as ($C_o = C_p + C_f + C_s$). Komori et al. (2013) measured high surface conductivity of ~ 10^{-1} S m^{-1} from hydrothermally altered rocks. A 10% smectite content can raise the surface conductivity of a rock matrix to 10^{-1} S m^{-1} (Revil et al. 2002; Komori et al. 2013) which easily accounts for low resistivity values in the Fang geothermal area. Because electrolyte conductivity of water in the fractures (calculated above) is < 1/4 the surface conductivity and the conductivity contributions are additive (0.022 S m^{-1} + 0.10 S m^{-1}) = 0.122 S m^{-1} (8.2 Ωm), the electrolyte contribution of the hot water in fractures is small and would not be detected in the presence of clay-bearing rock.

Within the temperature range 100–150 °C rock minerals are most susceptible to hydrothermal alteration and formation of high surface conductivity smectite. From 150 to 200 °C, the clay changes to a less conductive mixed phase of illite and smectite (Komori et al. 2013). Smectite is not observed in rocks > 200 °C, as it transitions to less conductive illite and chlorite (Essene and Peacor 1995). In the only well lithology record available from Fang, the FTGE-7 well, Ratanasthien et al. (1985) found montmorillonite (smectite) in the upper 23.5 m, and below that the dominant clay is illite and chlorite. Smectite is, therefore, the likely cause of low resistivity in the geothermal area and is probably associated with alteration about the main fracture systems and in the shallow zone of widespread seeps.

Pyrite is a common conductive mineral in geothermal areas and disseminated scarce pyrite is observed in gray shale at the Huai Han fluorite mine. Nelson and Van Voorhis (1983) and Rider (2002) show that disseminated pyrite > 5% significantly lowers rock resistivity from 50 to 100 Ωm to 2–20 Ωm. It is unknown if it is important in lowering the resistivity of rock in the Fang area because we do not have descriptions of well lithology.

Location, natural flow, and temperature of seeps and soil

Flow of the collective hot seeps was estimated by Nathan (1976) to be 30 l s^{-1} prior to development wells. Ramingwong et al. (1980) accurately monitored the natural thermal water discharge 1974–1979, and determined an average discharge of 20 l s^{-1} and fluctuations of about 5 l s^{-1}. The highest discharge of about 28 l s^{-1} occurred in the latter part of the rainy season. In February 2015, seeps were located with hand-held GPS units, temperatures measured, and individual seep flows were estimated (Fig. 23). The highest temperature seeps are distributed along a zone, 200 m long, trending with azimuth 340–350° (Fig. 15e). The zone is located 50 m west of the producing wells, FTGE-15, -7, sand-14. Seep temperatures in this zone range from 95.7 to 98.6 °C. The boiling point of the geothermal water at this elevation of 600 m is 99.3 °C. Another broader zone of 77–89 °C seeps trends 120 m to the east of this hot zone. Five small seeps 55.7–71.2 °C are scattered in a broad group 450 m to the NE of the hottest zone. A warm springs of 40 °C previously flowed from the N 40°W fault of the Huai San Fluorspar Mine, ~ 1.1 km SE of the main seep area (Shawe 1984; Hirukawa et al. 1987) (Table 3 and Fig. 13).

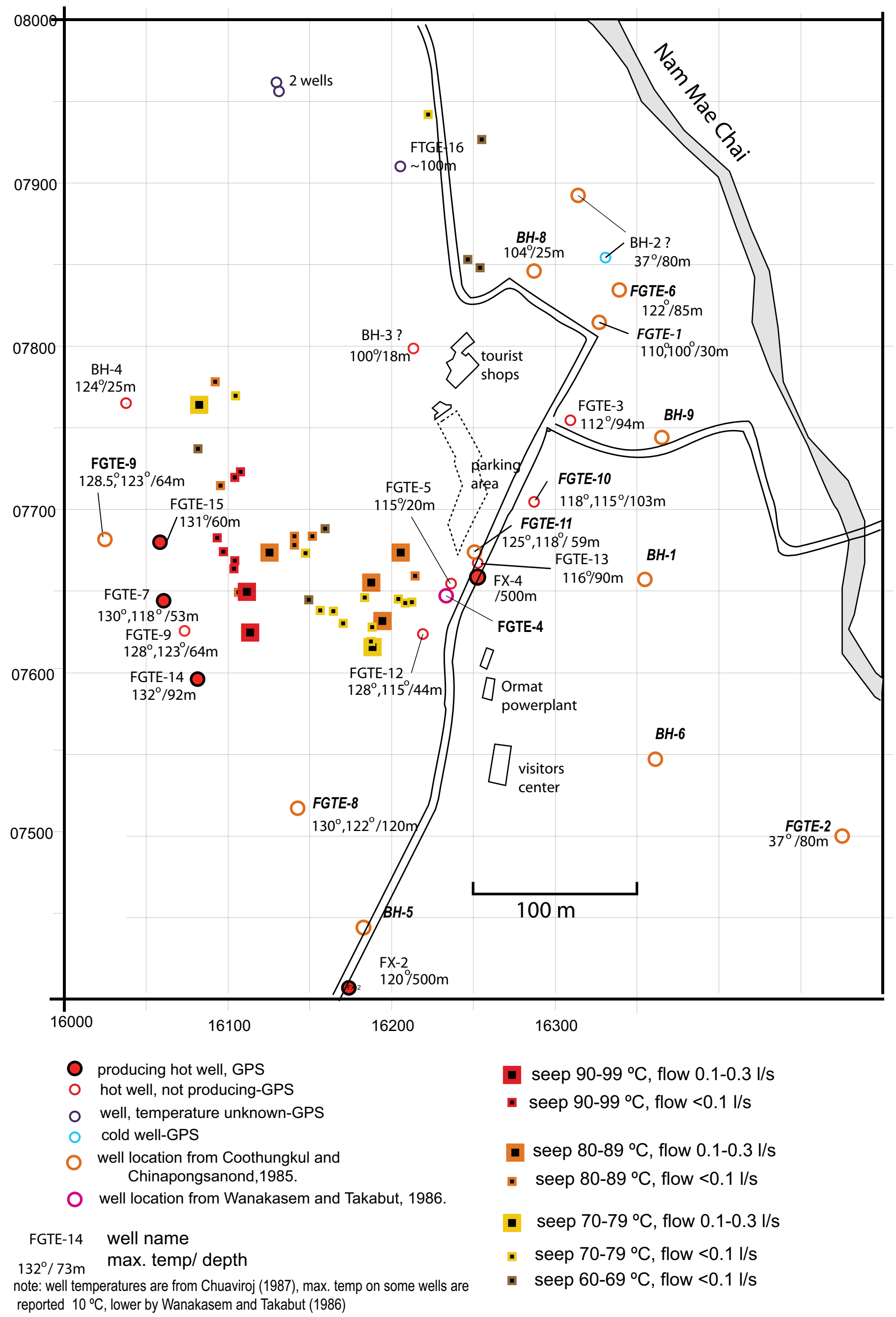

Fig. 23 Map showing locations of wells and hot spring seeps surveyed in 2015. Well locations listed in Table 1. Grid coordinates are UTM, WGS-84. Lower left corner (0516000E, 2207400N) corresponds to 99.152929ºE, 19.963050ºN

Our estimates of the largest individual seep flows ranged 0.1–0.3 l s^{-1}, at eight locations. Collectively, the warm water outflow of the hot springs stream at 0516150E, 2207550N was estimated at 10 l s^{-1} in February, 2015.

A soil temperature survey was made in 1980 at points spaced 100 m apart (Fig. 24). This simple inexpensive survey efficiently mapped the area of hot seeps and wells, and indicates that it could be extended with 50 m spacing to the unexplored area to the southwest beyond the FX-2 well. The 25 °C contour appears to identify the areas underlain by hot seeps and may serve as a guide to locating extensions of the fracture system to the southwest.

Structural geology

Tectonic framework

The Fang geothermal area lies at the west end of the active left-lateral Mae Chan fault where the strike-slip motion transfers to extension along N-S trending normal faults of the Fang basin. Morley (2007) discusses the late Cenozoic history of reversals in slip

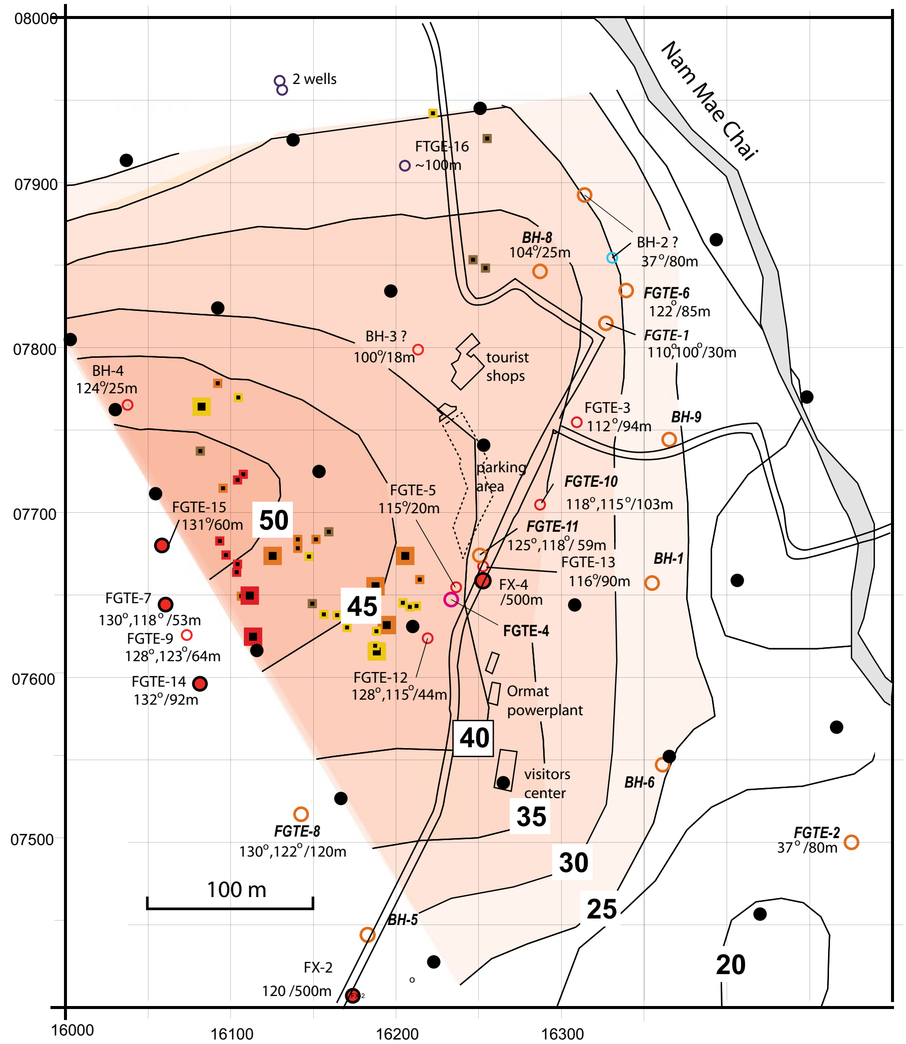

Fig. 24 Map showing 1-m depth temperature survey from Thienprasert and Raksaskulwong (1980) and reprinted with reference to well locations in Coothungkul and Chinapongsanond (1985). Temperature measurement point shown by black dots, well, and seep symbols explained in Fig. 23. The 25 °C contour effectively contains all hot wells and seeps and indicates a survey to the southwest may be useful to further exploration

direction on the Mae Chan fault and inversions recorded in the sediments and structures of the basin. The present tectonic state appears to be a hybrid of strike-slip and extension (Morley et al. 2011).

Because of deep weathering and thick vegetation, exposures of faulted rocks are scarce. Faults recognized in geological mapping are shown in Figs. 9, 12d, 25. None of these faults relate simply to the locations of hot springs in the crystalline rocks. The following discussion describes the observed structural features and how studies of fault architecture relate to the permeability of the crystalline rocks.

Mae Chan fault

The NE–SW-trending Mae Chan fault trends SW of the hot springs area. This active, left-lateral, strike-slip fault extends 200 km to the NE into Laos, but terminates to the southwest in the Fang basin (Uttamo et al. 2003, p. 96–99). Where exposed by a trench near Mae Ai, 12 km northeast of Fang, the fault dips 75°S and clearly offsets Quaternary sediment (Kosuwan et al. 2000). Offset streams and shutter ridges occur along the trace to the northeast (Fenton et al. 2003; Weldon 2015). In the Fang area, the fault is expressed physiographically as the linear edge of mountainous steep terrain to the northwest, with rolling hills to the southeast, and locally as saddles in ridges (Fig. 6). That change in topography is the contact between Paleozoic sedimentary rocks to the northwest and Cenozoic basin sediments to the southeast (Fig. 9). The fault contact is accurately located, but not exposed, in the bed of the Nam Mae Chai (river) at 0516800E, 2206480N, where black quartzite breccia associated with the base of the detachment is juxtaposed with sandy conglomerate (dipping 45° SW) of the Miocene Mae Fang Formation. The fault is clearly exposed as a vertical fault plane at the Huai Hian Reservoir (Fig. 25). The physiographic expression and these exposures show that the fault is composed of right-stepping segments at it western termination. The segments are 3–5 km long and the stepover zones are 0.5 km wide (Fig. 4). West of the hot springs, the MT profiles indicate a steeply dipping fault at depth (Fig. 22).

Doi Kia fault

Along the northwest basin margin, in the hot springs area, Paleozoic sedimentary rocks lie upon gneiss, foliated granite and mylonite believed to be Triassic in age. The contact generally strikes NE–SW, and dips 12° SE. Paleozoic rocks are not metamorphosed, and we find no evidence for an intrusive contact. A black quartzite breccia is commonly observed near the base of the Paleozoic rock, and is best exposed in the bed of the Nam Mae Chai (river) (0516750E, 2206660N). Also in the valley of the river, a 12-m-deep reservoir was excavated in 2015 into a massive, dark gray, gummy claystone with chunks of gray sheared quartzite (Fig. 14). In thin section, the quartzite is composed of granulated angular quartz grains less than 0.1 mm. We believe the claystone is a fault gouge near the base of the Paleozoic rocks. The dilemma of older rocks lying on younger rocks can be interpreted as a detachment fault that has displaced Paleozoic rocks on a low-angle normal fault over the younger crystalline rocks of Triassic age. Foliations of the lower plate granite and mylonite have moderately steep dips (28–50°), mostly to the west, and do not parallel the contact, indicating that the ductile deformation of the crystalline rock is not related to the detachment fault. Chaturongkawanich et al. (1980) named

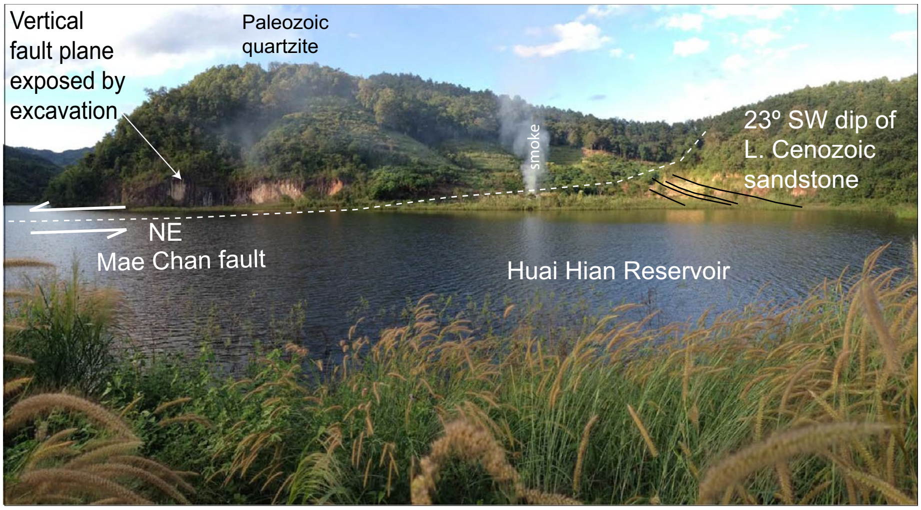

Fig. 25 Exposure of the Mae Chan fault at the reservoir of Huai Hian (creek), 3 km NE of the Fang geothermal area. Photo looking north from 0519800E, 2207300N

this irregular contact trace the Doi Kia fault, but did not interpret it as a detachment. Age of the detachment fault is uncertain, but Upton et al. (1997) interpret from apatite fission-track analysis that a massive unroofing of crystalline rocks of northwestern Thailand occurred in the late Oligocene. Late Oligocene is a reasonable age for the Doi Koi detachment.

Alignment of the hottest seeps in the hot springs area

The hottest seeps just west of well FTGE-15 are distributed over a distance of 100 meters, and align on a 165° azimuth (Figs. 15e, 23). Apparently this is a fracture trend in the crystalline rocks, different from the Mae Chan fault orientation and may be a deep conduit for upward percolating hot water. Another group of seeps align in an E–W direction with the low resistivity zone mapped by Coothungkul and Chinapongsanond (1985) (Fig. 18).

Huai San Mine fault

One km south of the hot springs area is the Huai San Fluorspar Mine. The mine pit is filled with water, and features described by Shawe (1984, p. 113–114) cannot now be observed. His report contains a sketch map of a N–NW fault that projects into the hot springs area (Fig. 13). The fault trends N 40° W, and forms a ~ 50-m-wide zone of sheared and brecciated Carboniferous shale and limestone bearing fluorspar. Dip of the fault and ore body are not stated in the report. Wall rocks on the NE side of the ore body are characterized by huge blocks of limestone embedded in deformed shale. The southeast wall of the ore body consists of deformed, clay-altered, fine-grained sedimentary rock that may be Cenozoic in age. Nearly horizontal grooves and slicken sides were conspicuous on the numerous shear surfaces in the open pit, indicating significant strike-slip movement along the fault zone. Shawe (1984) further notes that warm water is issued from a spring in the southeast part of ore body. Hirukawa et al. (1987) measured

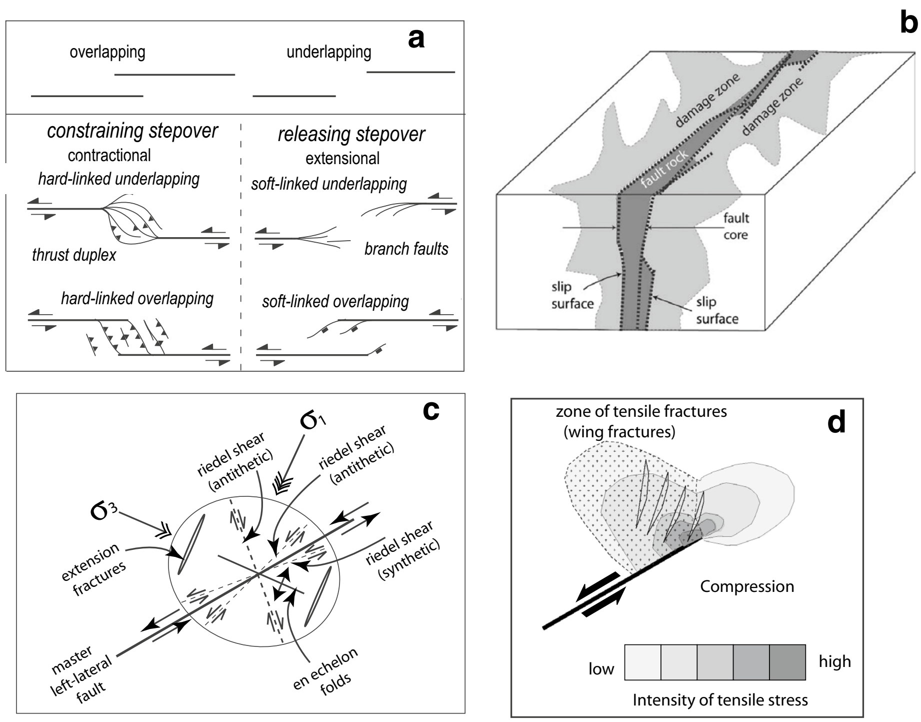

Fig. 26 Models of fracture systems associated with a left-lateral fault (one can use reverse images to view features of a right-lateral fault). **a** Attributes and features associated with stepover zones (after Micklethwaite et al. 2010). **b** Internal architecture of a strike-slip fault showing fault core of cataclastic rock, gouge, and slip surfaces, and the surrounding damage zone (after Aydin and Berrymore 2010); **c** Angular relations of fracture patterns along a left-lateral fault oriented with a 060° strike of the Mae Chan fault. Extensional (open) fractures should parallel the maximum principle stress, σ_1. The intermediate stress σ_2 is vertically down. The least principle stress is σ_3. Diagram is from Christie-Blick and Biddle (1985). **d** Zone of "tensile fractures" (open extensional fractures or cracks) expected at the tip of a left-lateral fault. Kim and Sanderson (2006) call this a zone of "wing cracks" because of the pattern over which they splay near the tip of the fault. For a system that propagates some distance from the fault, the term "wing fractures" may be more appropriate. Diagram based on concepts of fault tips in Gudmundsson (2000), Kim et al. (2004), Kim and Sanderson (2006), and Curewitz and Karson (1997). Pattern of tensile stress at the tip of a left-slip fault is from Reches and Lockner (1994)

the temperature of this spring at 40 °C and sampled the water for chemistry (Table 4). Limestone blocks were observed by us near the mine area. Exposed at the south end of the water-filled mine pit is a dark gray carbonaceous shale, with disseminated pyrite. Irregular vertical fractures strike 135° through this outcrop at 0516500E, 2206550N.

Normal fault east of hot springs

A high-angle normal fault is exposed in the east bank of the Nam Mae Chai (Fig. 12d). Black shale with silt lenses are drag folded down to the west. The fault plane is oriented with strike of 012°, and a dip of 83° to the west. Vertical slickenlines are on the down-dropped sandstone hanging-block face.

Deep (200 m +) crystalline rock boundary trending N-NE on MT images

In Figs. 21b, 22a, we show a white line bounding resistive crystalline rock from less resistive sedimentary rock to the east. The boundary dips about 50° SE and is observed on all MT model slices 200–1500 m deep, but not observed as a surface feature. The feature is unexplained except that it may be an older structure related to the western termination of the Mae Chan fault. Below ~ 1500 m depth the boundary appears to be vertical.

Ban Hua Fai fault

About 4 km south of the hot springs is a prominent N–S linear escarpment that appears to offset a terrace level of the Nam Mae Mao (river) 15 m, from the active floodplain to the east. The escarpment continues as a physiographic feature for another 7 km to the south. We name this feature the Ban Hua Fai fault after the village that sits upon the upthrown terrace level. The fault is believed to have Quaternary-aged displacement, but the fault plane is not exposed. Orientation is similar to the Mae Soon fault which forms the western boundary of the Fang basin (Figs. 2, 3, 4, 9). The scarp coincides with a normal fault observed on 3D seismic by Kongmongkhol et al. (2015). The Ban Hua Fai fault appears to be a normal fault and an expression of the termination of the Mae Chan fault as transtensional motion changes to the extensional boundary fault to the west.

Nam Mae Chai lineament

Previous publications show a N–NW fault through crystalline rock aligned with the Nam Mae Chai (river) north of the hot springs, which was called the Mae Chai fault (Chaturongkawanich et al. 1980; Amatyakul et al. 2016) (Fig. 6). No features, other than river alignment, have been found for this fault. Sound hard crystalline rock occurs in the river bed over a distance of 2 km north of the hot springs, with no observed breccia or fracture zones. The stream alignment does generally parallel the N–NW alignment of hottest seeps (Fig. 23) and also the NW striking fault observed by Shawe (1984) in the fluorspar mine (Fig. 13), but its significance is uncertain.

Fault architecture studies and permeability along faults

Faults and fractures are the permeable pathway for hydrothermal flow (Curewitz and Karson 1997; Micklethwaite et al. 2015; Faulds and Hinz 2015). The hot spring emanations and hot wells at Fang do not lie on an observed fault trace. Instead the geothermal manifestations are from crystalline rocks ~ 0.7 km north of the Mae Chan fault trace (Fig. 4). Fault zone architecture studies define fault core materials typically acting as low permeability barriers to flow, flanked by the damage zone of fractured permeable rock (Fig. 26b) (Mitchell and Faulkner 2009; Caine et al. 1996; Caine and Forster 1999; Aydin and Berryman 2015; Choi et al. 2016). The geothermal manifestation must be in a damage zone of high permeability and not in the fault core (i.e., not along the master fault trace: the Mae Chan fault).

The right-stepping segments of a left-slip fault indicates "restraining oversteps." Restraining steps show compression and uplift in the zone between the segments (Biddle and Christie-Blick 1985; Wakabayashi et al. 2004). A restraining stepover zone (in compression) does not indicate a zone of open extensional fractures needed to explain the upward flow of geothermal water. The Huai San fluorite mine fault has the NW–SE orientation of strike-slip movement consistent with an antithetic shear (Fig. 26c) in the restraining zone. The past history of the Mae Chan fault (Morley 2007) allows that fluorite mineralization may have occurred during a previous time of right-lateral motion when NW-oriented fractures were extensional rather than shear.

The Anderson (1951) model of fractures indicates that extension fractures should develop as oblique (40° counter-clockwise) to the master strike-slip fault, parallel to the maximum principle stress (Fig. 26c). Of interest here are open extensional fracture zones, called tensile fractures by Gudmundsson (2000), that propagate away from the fault core. En echelon extensional fractures form in the wall damage zone (Kim et al. 2004). Fault tips develop a damage zone of extensional fractures systems called wing fractures or cracks that curve away from the termination of a strike-slip fault (Kim and Sanderson 2006). We show a diagram of the zone of extensional wing fractures that might develop from the NE tip of the Mae Chan fault segment which lies 700 m south of well FX-2 (Fig. 26d). This geometry is a plausible explanation for open fractures in the crystalline rocks to the north. Earthquake aftershock distributions and the vertical extent of some mineral deposits show that fault damage zones have widths of several kilometers and typically extend to depths of several to 10 km providing permeable pathways for geothermal water (Micklethwaite et al. 2010). If wing fractures are the open fracture system, their dip may be 70–90° characteristic of high-angle normal faults shown as "secondary faults" of strike-slip faults by Price and Cosgrove (1990, Fig. 6. 27).

The normal fault exposed in the bank of the Nam Mae Chai (Fig. 12d) has a strike of 010° approximately consistent with 025° orientation of expected extension faulting. The mapped zone of low resistivity containing hot wells FTGE-7, -9, -14, -12, -6, and FX-4 (Fig. 18) trends 040° to 070° and may be the alignment of an open fracture system, but does not perfectly align with the expected 025° orientation. The 165° orientation of the zone containing the hottest seeps and the FX-2 and FGTE-8 hot wells (Fig. 23) is clearly oblique to the 060° strike of the Mae Chan fault, and does not align with the expected extension fault strike of 025° (Fig. 26c). These field observations and previous geophysics are too widely scattered to conclude the location of the fractures systems but we hope this structure discussion will help in interpreting future geophysical and drilling results. We do not believe the geothermal system percolates through the clayey sedimentary rock along and south of the Mae Chan fault or through the fault core itself. Rather, the crystalline rock north of the fault is the fault damage zone likely to hold open fractures necessary for deep permeability.

Geochemistry of the geothermal water

Ion chemistry of water sampled from the flowing wells and seeps is dominated with Na and HCO_3 (~ 120 ppm, ~ 100 ppm, respectively). pH values are high, ~ 9.1. Total dissolved solid values are relatively low 440 mg/L (EC is 550 μS cm^{-1}). Silica concentration is high at 170 mg l^{-1}. Fluoride concentration is 20 mg/L (Table 4). Singharajwarapan et al. (2012) calculated temperatures of 146 °C using conductive-cooling chalcedony geothermometry. Somewhat higher temperatures are obtained using other methods. Using the Giggenbach et al. (1994) plots of (log(Na/K) vs. log(SiO_2) and log(K^2/Mg) vs. log(SiO_2), Apollaro et al. (2015) obtain apparent equilibrium temperatures of 150 ± 5 °C. They further estimate the volume of the geothermal reservoir at Fang using $_3$H-based residence time and the natural flow rate. Evaluation of the geochemistry indicates that higher temperatures may be encountered in deeper drilling. The highest water temperatures measured are 131 °C in the 60-m deep FTGE-15 well (Table 1).

Locations of wells, drilling history, and power plant operation

In February, 2015 we obtained UTM coordinates on most of the early wells with the help of EGAT staff: Khun Pitak and Khun Inton (Table 1 and Fig. 23). Available maps showing locations of early wells are in publications by Wanakasem and Takabut (1986) and Coothungkul and Chinapongsanond (1985). Locations on those maps differ slightly (some are ± ~ 70 m) from the UTM Coordinates we establish. A number of wells could not be located: FGTE-2, FTGE-6, FTGE-10, BH-8, BH-11, FX-1, and FX-3. We hope to eventually obtain locations and well information from EGAT, as past drilling information is important to any further exploration.

Drilling of the geothermal system was started about 1982 in a cooperative agreement between the Electricity Generation Authority of Thailand (EGAT) and the Bureau de Recherches Geologiques et Minieres (BGRM) and Geowatt of France (Wanakasem and Takabut 1986). Twelve shallow wells with target depths of 100 m were drilled in the area of relatively low electrical resistivity (FTGE 1 through 12, Table 1). Eight slim holes were drilled by EGAT in 1984 to confirm the productive area of the shallow fractured reservoir. Productive flows were obtained from BH-3, BH-4, and BH-8 (Table 1). In late 1985 to early 1986, FTGE-14 and FTGE-15 were drilled to 73 m and 60 m, respectively, and obtained a combined flow of 22 l/s at 125 °C (Table 1). Production testing confirmed a reliable flow, and in December, 1989 the 300 kWe ORMAT power plant was put into operation (Korjedee 2000).

Further geological, electrical geophysics, and geochemistry studies were done in 1990 in cooperation with the French Environment and Energy Management Agency (ADEME) (Korjedee 2000), but we have not located those reports. These studies led to drilling of 4 wells: FX-1 through FX-4 wells with targets 500 m deep, currently the deepest wells in the system. FX-1 and FX-3 were non-productive and had bottomhole temperatures of 108 and 113 °C, respectively. Locations of these two wells are not known at time of writing. The FX-2 well was completed into as fracture at 270 m depth, and produced 7.0 l s^{-1} of 125 °C water. The FX-4 well was drilled to 500 m and completed into fractures at depths 268, 337, and 417 m and a bottomhole temperature of 130 °C (Korjedee 2000). The well produced 10 l s^{-1} (Ramingwong et al. 2000). FX-2 and FX-4 were connected to the power plant supply in 1996, and now produce 120 °C water (Khun Inton, personal communication, 2015). We have been unable to obtain logs, temperature profiles, or production tests from the wells. Table 1 is compiled from all information available at this time.

The FTGE-7 well was engineered to produce a 30-m-high "geyser" as a tourist attraction. The natural well flow is shut in every 30 min and the opened for 3 min to produce the spout that declines in height until shut in.

As of 2015, the generating system produced from 4 wells, FTGE-14, FTGE-15, FX-2, and FX-4 (original test flows and temperatures shown in Table 1). On a 2-week cycle, three wells flow to the power plant at any one time. One well is reamed and its flow, while reaming, is spilled to a stream to clean scaling. The collective flow from three wells is ~ 20 l s^{-1} of 110–115 °C water, somewhat less than earlier tests (Table 1) on account aging wells, perhaps cold-water leakage and transmission losses. Each well has a steam separator, and the steam released to the atmosphere without using the steam energy. The flow goes to the ORMAT binary plant rated at 300 kWe, and the spent geothermal water at 71–80 °C goes to a cooling pond, where it cools to ~ 27 °C, and then flows to the Nam Mae Chai (river), a stream that has a typical base flow of ~ 1500 l/s. Cool water (15–30 °C) is drawn from the river at a rate of up to 97 l/s to cool the working fluid in the cooling condenser. The cooling tower originally installed has not operated for many years. The power plant generates 115–250 kWe which varies with season.

Recommendations for future exploration and development

Further exploration of the Fang geothermal area

Good spatial resolution of the low resistivity area about the hot springs and producing wells is needed to determine if the hydrothermal alteration zones of fracture systems can be imaged. Detailed lateral DC resistivity profiles or a 3D resistivity survey should explore for deeper (50–200 m) hydrothermal alteration zones as indicators of the main fractures. The 500-m FX-2 well was drilled 200 m south of the known seepage area. We do not know the strategy of that 1995 FX-2 location, but it is at the south edge of the 1985 resistivity survey coverage, where low apparent resistivity (30–50 Ωm) is shown at the south ends of lines H-1 and H-6 (Fig. 20). Schlumberger sounding at R2 showed resistivity of ~ 30 Ωm below 30 m depth to a depth of about 100 m (Fig. 19). It should be relatively inexpensive to obtain detailed 2D profiling, or 3D coverage to a depth of 200 m, and interpret this survey with respect to seepage areas and previous drilling. DC methods can be employed rapidly and inexpensively with modern equipment and processing. MT and DC data can be integrated for a complete 3D model (W. Siripunvaraporn written communication, 2016). The survey should include the known geothermal area and be continued south to examine more closely anomalies detected by the MT survey.

The 1-m depth temperature survey of 1980 outlined the seep and producing well areas with the 25 °C contour (Fig. 24). This inexpensive survey method could be extended to the unexplored area to the southwest with 50 m spacing. Much of the productive geothermal area is outlined by existing wells (Fig. 23, Table 1), but drilling of shallow (< 100 m) temperature gradient wells will also be useful in exploring to the southwest of existing wells. It will be important to obtain good lithology logs and geophysical logs of future exploration wells. Although geochemistry indicates that higher reservoir temperatures > 146 °C may exist at depth, we have no guidance on location for a deep exploratory well, other than to drill into the known geothermal area over crystalline rocks, north of the Mae Chan fault.

Ways to increase water flows from wells and recommendation for further drilling

The wells, mostly 6-inch (14.3 cm) diameter, currently produce by natural flow. Some energy potential is lost by venting the steam. Greater flow could be obtained by pumping the wells and capturing hot fluids before fluid flash. These wells have never been pump tested, but could possibly be pumped at 30 l s^{-1}. The existing wells are old (> 20 years), have accumulated scale, and the casings have presumably partly deteriorated. Replacement wells may be necessary in the future. Pumping wells of 120 °C water at 55 l s^{-1} could produce ~2MWe with an upgraded modern power plant (Ormat Technologies, Inc., 2016).

Many successful exploratory wells in the past (temperatures > 110 °C) are shallow (< 150 m), so the cost of new shallow wells is not great. The problem has been to drill into a fracture system that will produce > 6 l/s. The area underlain by fracture systems bearing hot water appears to be overlain by low-resistivity altered granite to a depth of 25–50 m, as shown by past geophysical surveys and the recent MT survey of Amatyakul et al. (2016). Reports from past wells are not detailed, but fractures from 18 m to 417 m are reported from wells FTGE-14, FTGE-15, FX-2, and FX-4 (Table 1). A simple strategy is to drill new wells into the low-resistivity areas to depths less than 300 m, and obtain good information from cuttings, to temperature and caliper logs to locate the fracture systems. Well design should case and cement off cold-water inflows. A budget for multiple wells is necessary because these wells are exploring for steeply dipping open fractures capable of producing water, and some wells may not encounter a producing fracture. The wells are to some extent exploratory, but they should be drilled so that they can be reamed and completed as production wells. Diameter of wells should be large enough to set a > 6 l s^{-1} submersible pump. A 6-inch (14.3 cm) well will accommodate a high-temperature submersible pump with a capacity of ~ 30 l s^{-1}. An 8-inch (20.3 cm) well is preferred for casing-off colder flows and for working room.

It is recommended that the producing well system be designed for re-injection of the spent geothermal water in order to sustain pressure levels and temperature. Furthermore, the high fluoride content of this water (Table 4) may be a minor health hazard (c.f. Chuah et al. 2016), particularly if increased geothermal flows are discharged to the Nam Mae Chai (river) during seasonal low flows of ~ 250 l s^{-1}.

Conclusions

1. The Fang geothermal waters emanate from crystalline rocks 0.7 km north of the active, left-lateral, strike-slip Mae Chan fault. The permeable fractures are believed to be extensional "wing fractures" in crystalline rock related to the right-stepping segments at the west end of the Mae Chan fault. The Mae Chan fault core may have low permeability. The fault and Cenozoic sediments to the southeast of the fault are not considered to be drilling targets for further development.
2. At the hot springs, the Doi Kia detachment fault places Paleozoic sediments over crystalline rocks presumed to be Triassic in age, but the detachment is unrelated to the fracture system of the geothermal system.
3. Cenozoic sediments of the Fang basin lie SE of the Mae Chan fault. The near surface sediments are mostly coarse-clastic alluvial fan and fluvial sediment. Deeper rocks of the basin are the petroliferous shaly Mae Sot Formation which are a cause of low resistivity imaged by geophysical surveys.
4. The Fang geothermal heat is derived from the natural radioactive decay of K, Th, and U in the upper crustal crystalline rocks combined with heat flow from the lower crust and upper mantle. Northern Thailand geothermal systems are not associated with underlying magmatic systems. We estimate a heat flow of 94 mW m^{-2} using average values for measured heat flow from the sedimentary basin. This value of heat flow combined with a crystalline rock conductivity of 3.0 W m^{-1} $°C^{-1}$ suggests that the 130 °C temperatures arise from a depth of ~ 3 km depth.

5. DC and MT surveys indicate that the developed ~ 10-hectare geothermal area is underlain by a shallow zone (< 90 m deep) of low resistivity (< 30 Ωm) below which is resistive (> 100 Ωm) crystalline rock. Because the geothermal water at 130 °C has a relatively high resistivity of 5.6 Ωm, most of this low resistivity is caused by conductive clays of a hydrothermal alteration zone. Geophysical surveys should test their ability to image deeper fracture systems in the crystalline rock that may have similar conductive alteration zones.
6. Water from geothermal wells have low total dissolved solids of 440 mg/l (EC is 550μS cm^{-1}). Silica concentration is high at 170 ppm. Geothermometer calculations from water chemistry indicate reservoir temperatures of 140–150 °C, but hottest temperature from wells is 130 °C.
7. Hot seeps and wells cover a 10 hectare area. Temperatures of 130 °C have been measured in some wells 53–120 m deep. Success of the most southern 1995 well (FX-2), flow of 7 l s^{-1}, 125 °C water suggests that geophysical surveys and drilling should explore this southern area.
8. The Fang geothermal system currently flows ~ 20 l s^{-1} of 115–120C° water from 3 wells and generates 115–250 kWe from the 1989 ORMAT binary plant, rated at 300 kWe. Water is produced by natural flow, and some energy is lost by venting the steam. Flow could be increased by pumping and capturing hot fluids at depth before flashing. A flow of 55 l s^{-1} of 120°C water should produce ~2 MWe with an upgraded power plant.
9. All wells produce from fractures shallower than 417 m, so that new production wells need not be deeper than 500 m. New wells should be drilled to allow for a high-temperature-rated submersible pumps capable of 30 l s^{-1}. Production water from a generating facility should be re-injected to maintain temperature and pressure, and to minimize high fluoride (20 mg l^{-1}) outflow into surface waters.

Authors' contributions

FSS originated the project, directed the research, provided numerous unpublished reports, and made arrangements for fieldwork. PK conducted field measurements, sampling for chemistry, and assisted in field mapping. SHW conducted the field work, review of literature, and wrote the manuscript. All authors read and approved the final manuscript.

Author details

[1] Department of Geosciences, Boise State University, 1910 University Drive, Boise, ID 83725, USA. [2] Department of Geological Sciences, Chiang Mai University, Chiang Mai 50200, Thailand. [3] Present Address: Electricity Generating Authority of Thailand, Nonthaburi, Thailand.

Acknowledgements

We thank the Thailand Department of Alternative Energy and Development and the Department of Groundwater Resources for earlier support investigating Northern Thailand geothermal resources. We are appreciative of the many investigators of Fang over the past 37 years who have documented their findings in the many references.

Competing interests

The authors declare that they have no competing interests.

Availability of data and materials

Not applicable.

Consent for publication

Author's organizations consent for publication.

Ethics approval and consent to participate

Not applicable.

Received: 16 June 2017 Accepted: 14 December 2017
Published online: 06 February 2018

References

Aguilera R. Analysis of naturally fractured reservoirs from conventional well logs. J Petrol Technol. 1976;28:764–72.
Anderson EM. The dynamics of faulting and dyke formation with application to Britain. 2nd ed. Edinburgh: Oliver and Boyd; 1951.
Amatyakul P, Boonchaisuk S, Rung-Arunwan T, Vachiratienchai C, Wood SH, Pirarai K, Fuangswasdi A, Siripunvaraporn W. Exploring the shallow geothermal fluid reservoir of Fang geothermal system, Thailand via a 3-D magnetotelluric survey. Geothermics. 2016;64:516–26.
Apollaro C, Vespasiano G, De Rosa R, Marini L. Use of mean residence time and flowrate of thermal waters to evaluate the volume of reservoir water contributing to the natural discharge and the related geothermal reservoir volume. Application to northern Thailand hot springs. Geothermics. 2015;58:62–74.
Aydin A, Berryman JG. Analysis of the growth of strike-slip faults using effective medium theory. J Struct Geol. 2015;32:1629–42.
Barber AJ, Ridd MF, Crow MJ. The origin, movement and assembly of the pre-Tertiary tectonic units of Thailand. In: Ridd MF, Barber AJ, Crow MJ, editors. The Geology of Thailand. London: The Geological Society of London; 2011. p. 505–37.
Biddle KT, Christie-Blick N. Glossary-Strike-slip deformation, basin formation, and sedimentation. In: Biddle KT, Christie-Blick N, editors. Strike-slip deformation, basin formation, and sedimentation, vol. 37. Tulsa: SEPM Special Publication; 1985. p. 375–86.
Barr SM, Ratanasathein B, Breen D, Ramingwong T, Sertsrivanit S. Hot springs and geothermal gradients in northern Thailand. Geothermics. 1979;8:88–95.
Brace WF, Orange AS, Madden TR. The effect of pressure on the electrical resistivity of water-saturated crystalline rocks. J Geophys Res. 1965;70(22):5669–78.
Bodvarsson G. Temperature inversions in geothermal systems. Geoexploration. 1973;11:141–9.
Cabrera L, Roca E, Santanach P. Basin formation at the end of a strike-slip fault: the Cerdanya Basin (eastern Pyrenees). J Geol Soc Lond. 1988;145:261–8.
Caine JS, Evans JP, Forster CB. Fault zone architecture and permeability structure. Geology. 1996;24(11):1025–8.
Caine JS, Forster, CB. Fault zone architecture and fluid flow: insights from field data and numerical modeling. In: Faults and subsurface fluid flow in the shallow crust. 113 ed. American Geophysical Union Geophysical Monograph; 1999. p. 101–127.
Chaturongkawanich S, Wongwanich T, Chuaviroj S. Geology of Amphoe Fang, Changwat Chiang Mai, scale 1:15,000, geological survey division. Bangkok: Department of Mineral Resources; 1980. p. 49.
Choi J-H, Edwards P, Ko K, Kim Y-S. Definition and classification of fault damage zones: a review and a new methodological approach. Earth Sci Rev. 2016;152:70–87.
Christie-Blick N, Biddle KT. Deformation and basin formation along strike-slip faults. In: Biddle KT, Christie-Blick N, editors. Strike-slip deformation, basin formation, and sedimentation. No. 37. Tulsa: SEPM Special Publication; 1985. p. 1–34.
Chuaviroj S. Geothermal development in Thailand. In: Proceedings UNITAR/UNDP workshop on small geothermal schemes, Pisa. 1987. p. 155–171.
Chuah CJ, Lye HR, Ziegler AD, Wood SH, Kongpun C, Rajchagool S. Fluoride: a naturally-occurring health hazard in drinking-water resources of northern Thailand. Sci Total Environ. 2016;545–546:266–79.
Coothungkul V, Chinapongsanond P. Resistivity survey Fang geothermal project, Ban Pong Nam Ron, Amphoe Fang, Chiang Mai Province. Unpublished report to the Electricity Generating Authority of Thailand. 1985. p. 61.
Crow MJ. Radiometric ages of Thailand rocks: appendix. In: Ridd MF, Barber AJ, Crow MJ, editors. The Geology of Thailand. London: The Geological Society of London; 2011. p. 593–614.
Curewitz D, Karson JA. Structural settings of hydrothermal outflow: fracture permeability maintained by fault propagation and interaction. J Volcanol Geotherm Res. 1997;79:149–68.
Ensol Co., Ltd. Geothermal resources survey for promoting geothermal energy production and local industry: progress report No. 2. Report to the Thailand Department of Groundwater Resources from P&C Management, Ltd, Ensol Co., Ltd with technical support from the Groundwater Technology Service Center of Chiang Mai University. Bangkok, 8 chapters. 2015. (In Thai).
Essene EJ, Peacor DR. Clay mineral thermometry–A critical perspective. Clays Clay Miner. 1995;43(5):540–53.
Faulds JE, Hinz NH. Favorable tectonic and structural settings of geothermal systems in the Great Basin region, western USA: proxies for discovering blind geothermal systems. In: Proceedings world geothermal congress, Melbourne, Australia. 2015. p. 6.
Fenton CH, Charusiri P, Wood SH. Recent paleoseismic investigations in Northern Thailand. Annals of Geophysics 2003;46:957–81
Gabàs A, Macau A, Benjumea B, Queralt P, Ledo J, Figueras S, Marcuello A. Joint audio-magnetotelluric and passive seismic imaging of the Cerdanya Basin. Surv Geophys. 2016;37:897–921.
Gardiner NJ, Searle MP, Morley CK, Whitehouse MP, Spencer CJ, Robb LJ. The closure of Paleo-Tethys in eastern Myanmar and northern Thailand: new insight from zircon U–Pb and Hf isotope data. Gondwana Res. 2016;39:401–22. https://doi.org/10.1016/j.gr.2015.03.001.
Giao PH, Doungnoi K, Senkhamwong N, Srihiran S, 2011. Assessment of petroleum resources for the south Fang Basin: uncertainties and difficulties. The 4th petroleum forum: approaching to the 21st petroleum concession bidding round. http://www.dmf.go.th/cms/assets/1/16.pdf. Accessed 5 Feb 2015.
Giggenbach WF, Sheppard DS, Robinson BW, Stewart MK, Lyon GL. Geochemical structure and position of the Waiotapu geothermal field, New Zealand. Geothermics. 1994;23:599–644.

Gudmundsson A. Active fault zones and groundwater flow. Geophys Res Lett. 2000;27(18):2993–6.
Hirukawa T, Jarach W, Tangool W, Takashima I. Preliminary study on the geochemical characters of major geothermal fields in northern Thailand. Bull Geol Soc Jpn. 1987;38(1):21–32.
Imsamut S, and Krawchan V. Geology of Amphoe Fang Quadrangle (4848 IV) and Doi Pha Wok Quadrangle (4748 I), scale 1:50,000: Bureau of Geological Survey, Thailand Department of Mineral Resources, Technical Report No BGS 33/2548, 2005. p. 157 (in Thai).
Jaupart C, Mareschal J-C, Iarotsky L. Radiogenic heat production in the continental crust. Lithos. 2016;262:398–427.
Kawada K, Sasada M, Kanaya H. Preliminary study on heat generation from the granitic rocks in northern Thailand. Bull Geol Soc Jpn. 1987;38(1):7–12.
Kim Y-S, Peacock DCP, Sanderson DJ. Fault damage zones. J Struct Geol. 2004;26:503–17.
Kim Y-S, Sanderson DJ. Structural similarity and variety at the tips in a wide range of strike-slip faults: a review. Terra Nova. 2006;18:330–44.
Komori S, Kagiyama T, Takakura S, Ohsawa S, Mimura M, Mogi T. Effect of the hydrothermal alteration on the surface conductivity of rock matrix: comparative study between relatively-high and low temperature hydrothermal systems. J Volcanol Geoth Res. 2013;264:164–71.
Kongmongkhol S, Chantraprasert S. Inversion structures of the Fang Basin. In: Proceedings 5th conference on geology, geotechnology, and mineral resources of Indochina, Khon Kaen, Thailand. 23–24 Nov 2015. p. 4.
Korjedee T. Geothermal exploration and development in Thailand. In: Proceedings world geothermal congress 2000. Kyushu-Tohoku, Japan. 2002. p. 56–66. http://kgvrs.mine.kyushu-u.ac.jp/GVR%20report/No11/thailand.pdf. Accessed 5 Feb 2015.
Kosuwan S, Saithong P, Lumjuan A, Takashima, I, Charusiri P. Preliminary results of paleoseismic studies on the Mae Ai segment of the Mae Chan fault zone, Chiang Mai, Northern Thailand. In: Proceedings technical meeting on exodynamic geohazards in East and Southeast Asia. Committee for coastal and offshore geoscience programs in East and Southeast Asia (CCOP/TP27), 2000. p. 19–27.
Madon MBH. Analysis of tectonic subsidence and heat flow in the Malay Basin (offshore Peninsular Malaysia). Geol Soc Malays Bull. 1997;41:95–108.
Mann P. Global catalogue, classification and tectonic origins of restraining and releasing bends on active and ancient strike-slip fault systems. In: Cunningham WD, Mann P, editors. Tectonics of strike-slip restraining and releasing bends. Geological society. London: Special Publication; 2007. p. 13–142.
Mayo AL, Himes SA, Tingey DG. Self-organizing thermal fluid flow in fractured crystalline rock: a geochemical and theoretical approach to evaluating fluid flow in the southern Idaho batholith, USA. Hydrogeol J. 2014;22:25–45.
Micklethwaite S, Sheldon HA, Baker T. Active fault and shear processes and their implications for mineral deposit formation and discovery. J Struct Geol. 2010;32:151–65.
Micklethwaite S, Ford A, Witt W, Sheldon HA. The where and how of faults, fluid and permeability–insights from fault stepovers, scaling properties and gold mineralization. Geofluids. 2015;15:240–51.
Mitchell TM, Faulkner DR. The nature and origin of off-fault damage surrounding strike-slip fault zones with a wide range of displacements: a field study from the Atacama fault system, northern Chile. J Struct Geol. 2009;31:802–16.
Morley CK. Variations in late Cenozoic-recent strike-slip and oblique-extensional geometries, within Indochina: the influence of pre-existing fabrics. J Struct Geol. 2007;29:36–58.
Morley CK, Racey, A. Tertiary stratigraphy (Chapter 10). In Ridd MF, Barber AJ, Crow MJ, (eds). The Geology of Thailand, The Geological Society of London 2011. pp. 223–71.
Morley CK, Charusiri P, Watkinson IM. Structural geology of Thailand during the Cenozoic. In: Ridd MF, Barber AJ, Crow MJ, editors. The Geology of Thailand. London: The Geological Society of London; 2011. p. 273–334.
Morley CK, Westaway R. Subsidence in the super-deep Pattani and Malay basins of Southeast Asia: a coupled model incorporating lower-crustal flow in response to post-rift sediment loading. Basin Res. 2006;18:51–84.
Nathan S. Reconnaissance survey of the geothermal resources of northern Thailand: stage 1 reports (exploration). Unpublished report from Kingston Reynolds Thom & Allardice, Ltd, Aukland, New Zealand. 1976. p. 42.
Nelson PH, Van Voorhis GD. Estimation of sulfide content from induced polarization data. Geophysics. 1983;48(1):62–75.
Noisagool S, Boonchaisuk S, Pornsopin P, Siripunvaraporn W. Thailand's crustal properties from tele-seismic receiver function studies. Tectonophysics 2014;632:64–75.
Nuntajun R. Seismic stratigraphy of the Fang basin, Chiang Mai, Thailand. Chiang Mai Univ J Sci. 2009;36(1):77–82.
Ormat Technologies, Inc. Fang status and future expansion - presentation to the Electricity Generating Authority of Thailand, December 22, 2016.
Owens, L. Initial assessments of high potential sites in northern Thailand. Unpublished report of Ormat Corporation, Reno, Nevada. 2012. p. 8.
Petersen HI, Foopatthanakamol A, Ratanasthien B. Petroleum potential, thermal maturity and the oil window of oil shales and coals in Cenozoic Rift basins, Central and Northern Thailand. Journal of Petroleum Geology 2006;29 (4):337–60.
Petford N, Cruden AR, McCaffrey KJW, Vigneresse J-L. Granite magma formation, transport, and emplacement in the earth's crust. Nature. 2000;408:669–73.
Price NJ, Cosgrove JW. Analysis of Geological Structures. Cambridge: Cambridge University Press; 1990. p. 502.
Racey A. Petroleum Geology (Chapter 13) In Geology of Thailand In: M.F. Ridd, A.J. Barber and M.A. Crow (eds) Geology of Thailand. Geological Society of London Special Publication 2011. pp. 251–392.
Ramingwong T, Ratanasthien B, Wattananikorn K, Tantisukrit C, Lerdthusunsee S, Thanasutipitak T, Pitragool S. Geothermal resources of northern Thailand: San Kampaeng, Fang, and Mae Chan geothermal systems. Final Report submitted to the Electricity Generating Authority of Thailand. 1980. p. 171.
Ramingwong T, Lertsrimongkol S, Asnachinda P, Praserdvigai S. Update on Thailand geothermal energy research and development. In: Proceedings world geothermal congress, Kyushu-Tohoku, Japan. 2000. p. 377–386.
Ratanasthien B, Panjasawatwong Y, Yaowanoiyothin W, Lerdthusnee S, Haraluck M. Water qualities of geothermal fluids from San Kamphaeng and Fang geothermal systems. Final Report to Electricity Generating Authority of Thailand. 1985. p. 249.
Reches Z, Lockner DA. Nucleation and growth of faults in brittle rock. J Geophys Res. 1994;99(B9):18159–73.

Revil A, Hermitte D, Spangenberg E, Cochemé JJ. Electrical properties of zeolitized volcaniclastic materials. J Geophys Res. 2002. https://doi.org/10.1029/2001jb000599.
Revil A, Cuttler S, Karaoulis M, Zhoa J, Raynolds B, Batzle M. The plumbing system of the Pagosa thermal springs, Colorado: application of geologically constrained geophysical inversion and data fusion. J Volcanol Geotherm Res. 2015;299:1–18.
Ridd MF. East flank of the Sibumasu block in NW Thailand and Myanmar and its possible northward continuation into Yunnan: a review and suggested tectono-stratigraphic interpretation. J Asian Earth Sci. 2015;104:160–74.
Ridd MF, Barber AJ, Crow MJ. Introduction to the geology of Thailand. In: Ridd MF, Barber AJ, Crow MJ, editors. The Geology of Thailand. London: The Geological Society of London; 2011. p. 1–17.
Rider M. The Geological interpretation of well logs. 2nd ed. Sutherland: Rider-French Consulting Ltd; 2002. p. 280.
Ross SH. Geothermal potential of Idaho. Idaho Bureau of Mines and Geology Pamphlet 150. 1971. http://www.idahogeology.org/PDF/Pamphlets_(P)/P-150.pdf. Accessed 3 Dec 2017.
Sen PN, Goode PA. Influence of temperature on electrical conductivity in shaly sands. Geophysics. 1992;57:89–96.
Settakul N. Fang oilfield development. Walailak J Sci Technol. 2009;6(1):1–15.
Shawe DR. Geology and mineral deposits of Thailand. US geological survey open-file report. 1984. p. 84–403
Singharajwarapan FS, Wood SH, Prommakorn N, Owens L. Northern Thailand geothermal resources and development: a review and 2012 update. Trans Geotherm Resour Counc. 2012;2012(36):787–91.
Siripunvaraporn W. MT Data report: Fang. Unpublished report to the Thailand Department of Groundwater Resources from Department of Physics, Mahidol University, Bangkok. 2015. pp. 24.
Thailand Department of Mineral Resources. Lexicon of stratigraphic names. Thailand: Thailand Department of Mineral Resources; 2013. p. 262.
Thienprasert A, Raksaskulwong M. Heat flow in northern Thailand. Tectonophysics. 1984;103:217–33.
Thienprasert A, Raksaskulwong M. Fang geothermal energy project: Report on geophysical investigation: One meter depth temperature survey. Unpublished report to Electricity Generating Authority of Thailand from the Thailand Department of Mineral Resources 1980. pp. 15.
Upton DR, Bristow CS, Hurford AJ, Carter A. Tertiary tectonic denudation of northwestern Thailand: provisional results from apatite fission-track analysis. International Conference on Stratigraphy and Tectonic Evolution of Southeast Asia and the South Pacific. Bangkok, Thailand, 19–12 August, 1997. p. 421–431.
Uttamo W, Elders C, Nichols G. Relationships between Cenozoic strike-slip faulting and basin opening in northern Thailand. In: Storti F, Holdsworth RE, Salvini F, editors. Intraplate strike-slip deformation belts. Geological Society. London: Special Publications; 2003. p. 89–108.
von Braun E, and Hahn L. Geological map of northern Thailand, Sheet (Chiang Rai) 2, 1:250,000. Federal Institute for Geology and Natural Resources (Federal Republic of Germany), Stuttgart. 1981. http://www.dmr.go.th/ewtadmin/ewt/dmr_web/main.php?filename=Download_geo_En. Accessed Oct 15 2016.
Wakabayashi J, Hengesh JV, Sawyer TL. Four-dimensional transform fault processes: progressive evolution of step-overs and bends. Tectonophysics. 2004;392:279–301.
Wanakasem S, Takabut K. Present status of Fang geothermal project, Thailand. Geothermics. 1986;15:583–7.
Waples DW. A new model for heat flow in extensional basins: radiogenic heat, asthenospheric heat and the McKenzie model. Nat Resour Res. 2001;10(3):227–38.
Weldon R. How often does the Mae Chan fault generate large earthquakes? Powerpoint presentation to the northern Thai Study Group-Alliance Francaise, Chiang Mai, 2015. http://www.intgcm.thehostserver.com/diary.html. Accessed 5 Jan 2016.
Wood SH, Pirarai K, Fuangswasdi A, Kaenteo W, Waibel A, Singharajwarapan FS. Muang Rae geothermal system: drilling and borehole geophysics, 1000-m core hole into granitic rock, Amphoe Pai, Mae Hong Son Province, Northern Thailand. Geotherm Resour Counc Trans. 2016;40:659–70.
Wood SH, Singharajwarapan FS. Geothermal systems of northern Thailand and their association with faults active during the Quaternary. Geotherm Resour Counc Trans. 2014;38:607–15.
Ziagos JP, Blackwell DD. A model for the transient temperature effects of horizontal fluid flow in geothermal waters. J Volcanol Geoth Res. 1986;27:371–97.